Title	Reaction mechanism of L-Iactate oxidase based on X-ray structural analysis
Author(s)	Umena, Yasufumi
Citation	大阪大学, 2007, 博士論文
Version Type	VoR
URL	https://hdl.handle.net/11094/23006
rights	
Note	

Reaction mechanism of L-lactate oxidase

based on X-ray structural analysis

A Doctoral Thesis

by

Yasufumi Umena

Submitted to the Graduate School of Science

Osaka University

JAPAN

May, 2007

Reaction mechanism of L-lactate oxidase

based on X-ray structural analysis

（X線結晶構造に基づくL-乳酸酸化酵素の反応メカニズムの研究）

A doctoral thesis

By

Yasufumi UMENA

Submitted to the Graduate School of Science

Osaka University

JAPAN

May, 2007

ACKNOWLEDGEMENT

I also thank all members of Laboratory of Protein Crystallography in Institute for Protein Research, Osaka University and Laboratory of Neutron Scattering Science in Research Reactor Institute, Kyoto University.

Finally, I deeply thank to my parents, Yoshiaki and Tomoko, for appreciating and supporting me.

<div align="right">

梅名泰史

Yasufumi Umena
</div>

May, 2007

Table of contents

ABBREVIATIONS

C/N-terminus	carboxyl/amino-terminus
DEAE	diethylaminoethyl
ES complex	enzyme-substrate complex
FMN	flavin mononucleotide
FB2	flavocytochrome b_2
GOX	glycolate oxidase
k_{cat}	turnover number
K_m	Michaelis constant
KPi	potassium phosphate buffer
NAD	nicotinamide adenine dinucleotide
NCS	non-crystallographic symmetry
LCHAO	long-chain hydroxy acid oxidase
LMO	L-lactate monooxygenase
LOX	L-lactate oxidase
PEG	polyethylene glycol
pK_a	acid dissociation constant
r.m.s.	root mean square

CHAPTER 1: INTRODUCTION

1.1 Overview of α-hydroxy acid oxidase

L-lactate oxidase (LOX) belongs to a flavin mononucleotide (FMN) dependent α-hydroxy acid dehydrogenease family. The enzymes of the family do not use a nicotinamide adenine dinucleotide (NAD) as an electron-receptor like lactate dehydrogenase (LDH; EC: 1.1.1.27). It is generally agreed that the catalytic reaction of FMN dependent α-hydroxy acid dehydrogenases consists of two steps. The first step is a reductive half-reaction; the dehydrogenation from α-hydroxy acid to keto acids coupled with reduction of FMN. The second step is an oxidative half-reaction; a molecular oxygen is reduced to a hydrogen peroxide coupled with FMN oxidation.

The well known members of this family enzymes are, flavocytochrome b_2 (FB2) from *Yeast* (Xia ,Z., et al., 1987; Lindqvist, Y., et al., 1991), L-lactate monooxygenase (LMO) from *S. smegmatis* (Lederer, F., 1991; Ghisla, S., et al., 1991), glycolate oxidase (GOX) from *spinach*(Lindqvist, Y., et al., 1991), L-mandelate dehydrogenease from *Rhodotorula graminis* (Smekal, O., et al., 1993) and long-chain hydroxy acid oxidase (LCHAO) from *Rattus norvegicus* (Diep Le, K. H., et al., 1991). Among these family enzymes, FB2 (Xia-Z, K, et al., 1987), GOX (Lindqvist, Y. 1989) and LCHAO (Cunane,

1

L. M., et al., 2005) have been determined by X-ray crystallography (PDB code: FB2; 1FCB, GOX; 1AL7, 1GOX and LCHAO; 1TB3). The comparison of these structures reveals that these proteins have a common fold consisting of eight α-helices and eight β-strands in typical α/β barrel arrangement which is usually called "TIM barrel" motif. Additionally, these enzymes possess a set of conserved amino acid residues which are located in very similar spatial position around FMN molecule.

FB2 catalyzes oxidation of L-lactate to pyruvate as LOX does, but it has a different oxidative half-reaction from other family enzymes, because it has a heme as an electron receptor. LCHAO preferably catalyzes a long chain hydroxy acid. GOX has the highest similarity to LOX in amino-acid sequence with 35.4 % homology, but it catalyzes a glycolate, which does not contain a chiral atom in contrast to L-lactate. The multi-sequence alignment of three enzymes is shown in **Fig. 1.**

Two different mechanisms of the reductive half-reaction proposed from structural and functional research of these enzymes were presented by Fitzpatrick, P. F. (2004). The catalytic reaction mechanism of α-hydroxyl acid oxidase has been studied well based on the structure of FB2. Two possible mechanisms of dehydrogenation in the reductive half-reaction are the carbanion mechanism (Urban, P. et al., 1988; Dubois, J., et al., 1990) and the hydride transfer mechanism (Gondry, M., et al., 2001).

In the carbanion mechanism the active site base

2

residue (histidine) initially abstracts the α-proton of chiral center (Cα-H) of a substrate and the intermediary carbanion is oxidized to keto acid with transferring electrons to FMN. On the other hand, in the hydride transfer mechanism the hydroxyl-group proton (Cα-OH) is abstracted by the active site base residue (histidine) and the α-proton is transferred to the flavin N5 atom as a hydride (**Fig. 2**).

FB2 structure which is reasonable model as well as the LOX has been generally used for the analysis of the reaction mechanism of α-hydroxy acid oxidase. However, it is under debate which mechanism is applied to the dehydrogenation reaction.
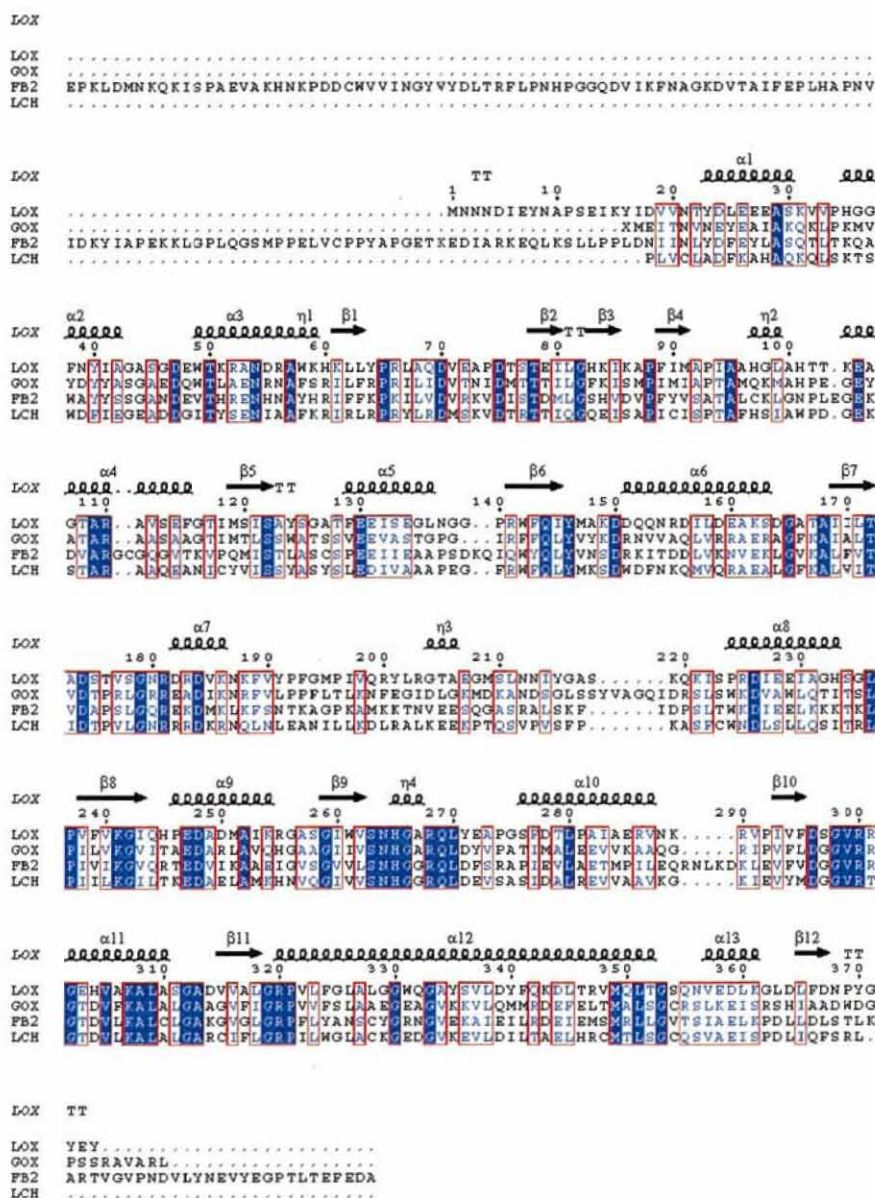
Fig. 1 Multi-sequence alignments of LOX and other family enzymes whose X-ray structures have been determined. The alignments were performed by the *ClustalW* program. LOX: L-lactate oxidase, GOX: glycolate oxidase, FB2: Flavocytochrome B2, LCH: long-chain hydroxyl acid oxidase.

4
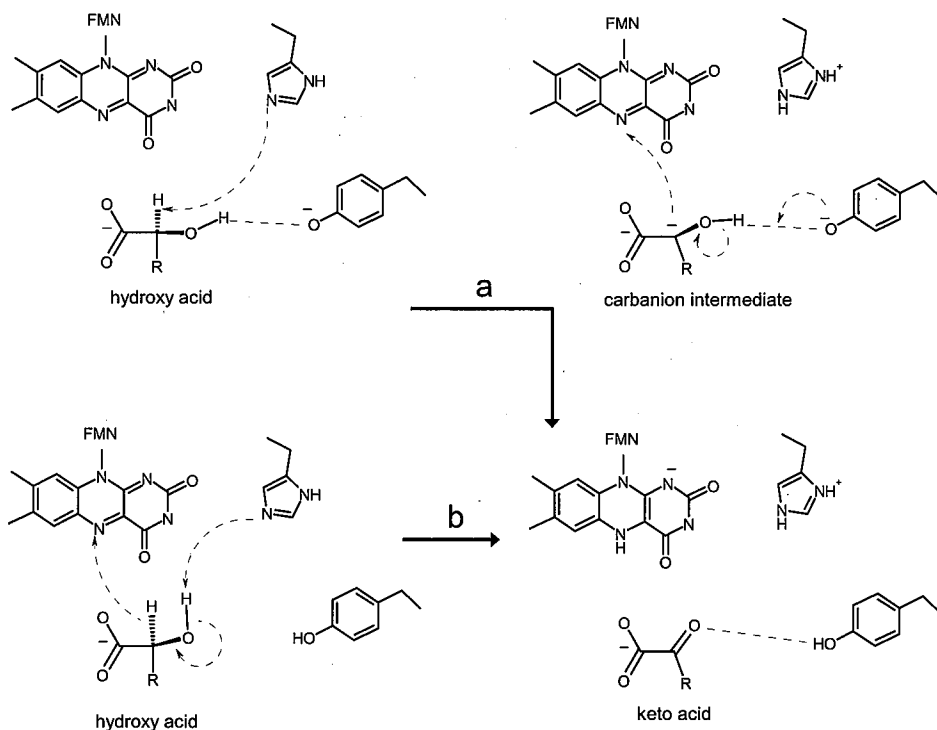
Fig. 2 The reaction mechanism schemes about the oxidation of the α-hydroxy acid to keto acid. The pathway (a) is called carbanion mechanism where a carbanion intermediate is yielded, and the pathway (b) is called hydride transfer mechanism.

1.2 Overview of L-lactate oxidase

L-lactate oxidase (LOX), a member of flavoenzymes, catalyzes the oxidation of α-hydroxy acids to keto acids with two-electron reduction of flavin mononucleotide (FMN). It oxidizes L-lactate yielding a pyruvate, and reduces a dioxygen molecule to a hydrogen peroxide (**Fig. 3**). LOX's molecular weight is 41 kDa and it has a flavin mononucleotide (FMN) molecule as a cofactor on each subunit without any covalent bond with the enzyme. It forms a tetramer in solution at neutral pH (Dancan, D.J., et al., 1989). It has been isolated from some microbial families; *Streptococcus faecalis*, *Pediococcus* and *Aerococcus viridans* (Sergio, A., et al., 2002). LOX from *Aerococcus viridnas* was used in this study.

The reaction mechanism of FMN dependent α-hydroxy acid dehydrogeneases are still in debate as stated before. LOX has highly specificity with L-lactate (Dancan, J. D., et al., 1989). They have reported that D-lactate, glycolate and D,L-2-hydroxybutylrate were not catalyzed by the LOX, but they become to be competitive inhibitors. Moreover, other report discusses that its catalytic activity for bulky substrate (long-chain hydroxy acid and aromatic hydroxy acid) is low (Yorita, K., et al., 1996).

Compared with FB2 or LMO, LOX has some advantages for studying the catalytic mechanism of lactate oxidation. In this, the components of the reaction center are simpler than that of FB2, and the reaction

6

scheme in oxidative half-reaction is shorter than that of LMO. FB2 transfers electrons to another cofactor, a heme molecule (protoporphyrin), at the active site cavity and LMO has an additional catalytic pathway from pyruvate to acetate with addition of H_2O. It is given in **Fig. 3**.

Therefore, the utilization of LOX is suitable for the study of L-lactate oxidase. Furthermore, the structural and functional studies of LOX may solve the underlying problem of the FMN dependant catalytic mechanism of α-hydroxy acid.

Reductive half-reaction

L-lactate   LOX$_{ox}$-L-lactate ⟶ LOX$_{red}$-pyruvate   pyruvate

LOX$_{ox}$ LOX$_{red}$

H$_2$O$_2$ O$_2$

Oxidative half-reaction
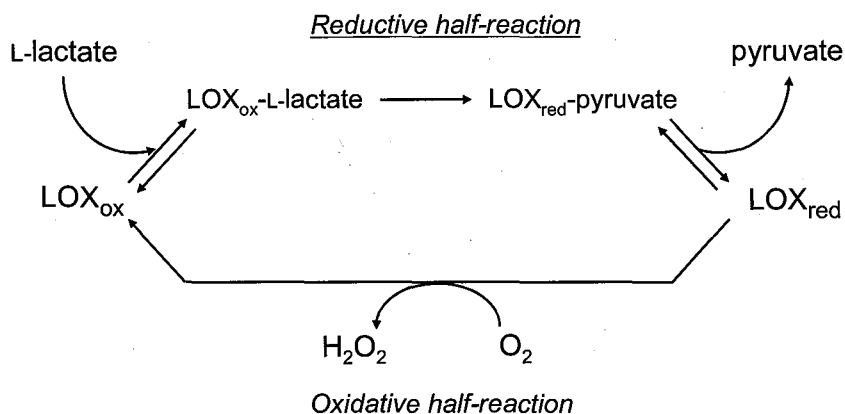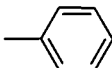
Fig. 3 The reaction pathway of L-lactate oxidase. The dehydrogenation of a lactate produces a pyruvate in reductive half-reaction (upper pathway) and oxidized LOX is generated in the oxidative half-reaction (below pathway).

Table 1 Substrate molecules of α-hydroxy acid oxidase

substrate molecule	R-CαH(OH)-COOH (R: substituent)
glycolate	—H
lactate	—CH$_3$
mandelate	—⟨benzene ring⟩
2-hydroxy butyrate	—CH$_2$—CH$_3$

8

1.3 LOX-pyruvate complex as an ES complex mode

A pyruvate is a product of the catalytic reaction by LOX, and it is released from the reduced LOX in reductive half-reaction (Maeda-Yorita, K., et al., 1995). Although the pyruvate can form a complex with the oxidized LOX when it is added in large excess than the enzyme, the complex is inactive and not included in the reaction cycle given in **Fig. 3**.

Since a pyruvate and a lactate molecules share methyl and carboxyl groups, the pyruvate was used as a substrate analog to prepare a mimic model of an enzyme-substrate (ES) complex. Thus, the oxidized LOX-pyruvate complex is not an enzyme-product complex in the reaction cycle but a model of an ES complex in the present study.

A redox state of the enzyme was confirmed by absorption spectrum and a structure of the authentic ES complex, the oxidized LOX-lactate complex, was predicted from the structure of the oxidized LOX-pyruvate complex in this study.

1.4 The purpose and brief summary of the study

Flavoprotein function must come from the fine-tuned mechanism based on the interaction of a substrate with a flavin and the adjacent amino acid residues. It is very important to understand the relationship between structure and biological function in an atomic resolution. A structural study of LOX has been initiated to understand not only functional mechanisms of LOX itself but also flavoproteins.

In the present study, I focused the structural studies of LOX on the oxidation mechanism of α-hydroxy acid depending FMN. Two possible mechanisms, the carbanion mechanism and the hydride transfer mechanism, have been proposed for the reductive half-reaction of the reaction cycle (**Fig. 3**) as described before. The primary purpose of the study is to determine whether the reaction of LOX proceed in the carbanion mechanism or in the hydride transfer mechanism. Another purpose of the present study is to deepen discussions on two possible mechanisms for FMN dependent α-hydroxy acid dehydrogenease family.

Additionally, in a future purpose for the industrial development, LOX from *Aerococcus viridans* is expected to be used as the receptor in biosensor applications developed to determine blood lactate level. But LOX is unstable for using as biosensors in a long-term. The detailed three-dimensional structure will aid in assessing how the enzyme may be stabilized and reaction

10

rate increased.

The first structure of native LOX (PDB code; 2DU2) was determined at 2.0 Å resolution, and showed some identical arrangements of the active site residues and some different features compared with other family enzymes such as FB2, GOX and LCHAO. The structure of LOX-pyruvate complex was determined at 1.9 Å resolution to elucidate the interaction between enzyme and substrate. By simulating a substrate (L-lactate) structure in the active site, the characteristic interactions of enzyme and substrate in LOX were revealed. The simulated structure of ES complex showed a characteristic substrate-binding motif and the substrate specificity of LOX. The ES complex structure indicated that the hydride transfer mechanism was preferable for the scheme of reductive half-reaction in comparison with the alternative mechanism.

CHAPTER 2: MATERIAL AND METHOD

2.1 Expression and Purification

LOX was expressed in *E.coli*. The transformed *E.coli* cells (350 g) were obtained from a 150 L fermentor culture incubated for 3h at 298 K with 4 L of 0.02 M potassium phosphate buffer (KPi buffer) adjusted at pH 7.0, containing 0.1 % lysozyme, 2 mM EDTA and 0.1 % Triton X-100. After centrifuge to remove cell debris, LOX was collected by acetone fractionation at 283 K. The acetone precipitate was dissolved in 0.02 M KPi buffer (pH 7.0), and was fractionated by precipitation with $(NH_4)_2SO_4$ between 0.38 M and 0.61 M. The precipitate was dissolved in 0.02 M KPi buffer (pH 7.0), and excess salts were removed by passing through a G-25 gel-filtration column equilibrated with the same buffer.

The supernatant was loaded on a DEAE sephadex A-50 column equilibrated. The column was washed with the same buffer and then was subjected to a gradient of 0 to 0.5 M KCl. The enzyme was eluted at approximately 0.3 M KCl. After concentrating by ultra-filtration and equilibration with 0.02 M KPi buffer (pH 7.0), pure enzyme was fractionated on a Sephadex G-150 column.

It was homogeneous on SDS-PAGE migrating at a position corresponding to a molecular mass of approximately 40 kDa. Purified protein was stored as a

lyophilized powder containing 70-80 % sucrose. When we used it for the crystallization, the lyophilized powder was dissolved in 0.05 M Tris buffer (pH 8.0) and the enzymes was separated from sucrose and other salts by passage through a sephacryl S-200HR column.

For the crystallization, the sample was concentrated to 20 mg/ml in 0.05 M Tris buffer at pH 8.0. The protein concentration was determined by the absorption coefficient at 456 nm of 11.0 x 10^3 $M^{-1}cm^{-1}$ and molecular weight of 41 kDa (Maeda-Yorita et al., 1995).

2.2 Absorption spectrum analysis

Absorption spectra were measured for four different states of the enzyme; a native enzyme, a mixture of enzyme with pyruvate, an oxidized enzyme and a reduced enzyme.

These enzyme solutions were adjusted at final concentration of 1 mg/ml with 0.05 M Tris buffer (pH8.0). The oxidized sample was prepared by mixing 0.01 M *Para*-benzoquinone solution (final concentration: 1 mM) and reduced sample was prepared by mixing 1 M L-lactate solution (final concentration: 0.1 M). The sample mixed with pyruvate was prepared at final concentration of 0.1 M and this sample was the same one as that used for crystallization. These additive reagents, *para*-benzoquinone, L-lactate and pyruvate, were added to the sample solution just before measuring the spectrums. The pH values of these three mixed samples were maintained at pH 8.0. The concentrations of these additive reagents were excessively higher than that of the enzyme.

The absorption spectra were measured at room temperature (293 K) using the spectrometer Hitachi U-2010 and they were collected in the range of 350-800 nm by subtracting the base-line absorbance which was measured without enzyme. The observed spectra were shown in **Fig. 4**.
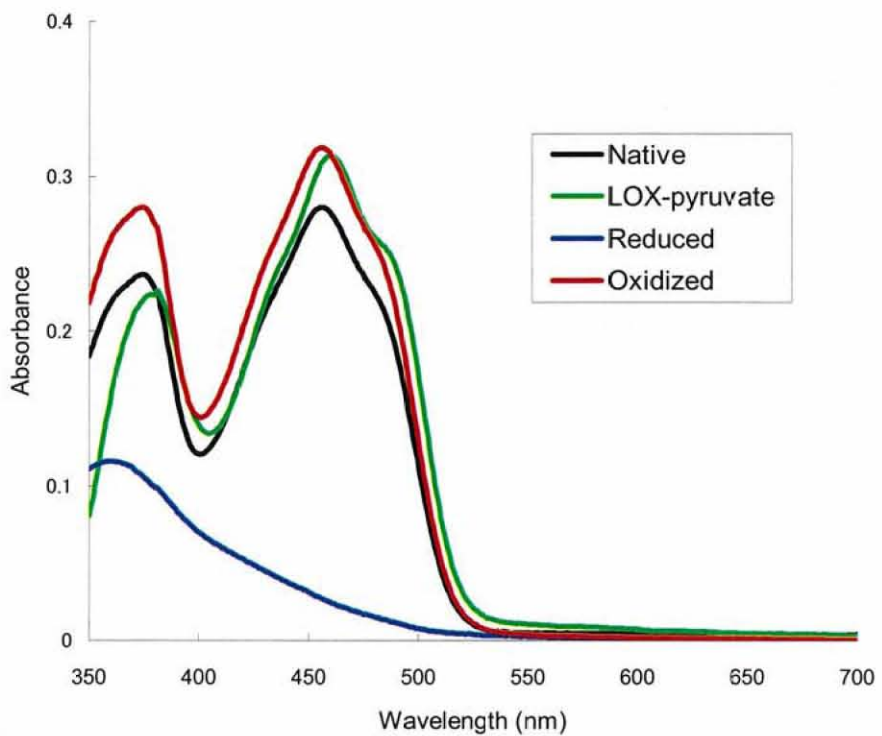
14

Fig. 4 The absorbance spectra of four samples in
the range of 350-800 nm: a red line, the sample
oxidized by 1 mM *para*-benzoquinone; a blue line, the
sample reduced by a substrate of 0.1 M L-lactate;
a green line, the sample mixed with 0.1 M pyruvate;
and a black line, additive-free native sample.

15

2.3 Crystallization

Native LOX

Firstly, LOX crystal was crystallized at 288 K from a solution containing 10 % polyethylene glycol (PEG) 6000, 0.1 M MES buffer (pH 6.0) at a protein concentration of 16 mg/ml (Morimoto et al., 1998). But this crystal was not suitable for solving the crystal structure.

Searching various crystallization conditions using sitting-drop vapor diffusion method, we successfully found the new condition giving crystals suitable for the crystal structural analysis. 2 µl protein solution concentrated to 15 mg/ml was mixed with 2 µl reservoir solution containing 18% PEG 4000, 0.1 M Tris buffer at pH 8.0, 0.2 M Lithium sulfate and the 4 µl droplet was equilibrated against 50 µl reservoir solution at 293 K. A few days later, there was no crystal and then the reservoir solution was changed to the solution containing a higher PEG 4000 concentration of 24%. Crystals were grown to rod shape with 0.1 mm length within one week.

It was important to grow the crystal that the PEG concentration was changed from 18 % to 24 % after initial equilibration with 18 % PEG for a few days. The crystals grew to more than 0.1 mm length for the operation and this size was suitable for X-ray data-collection experiment. The crystal is showed in **Fig. 5** (a).

LOX-pyruvate complex

The complex of LOX and pyruvate were prepared by the following method. Firstly, LOX was mixed with the solution which consisted of 0.2 M pyruvate, 0.05 M Tris buffer at pH 8.0. The concentrations of the enzyme and pyruvate were 10 mg/ml and 0.1 M, respectively. Next, the sample was incubated at 4 ℃ overnight. Then, the LOX-pyruvate complex was equilibrated against a solution containing 25 % PEG 3350, 0.2 M ammonium acetate, Bis-Tris buffer at pH 6.5 by vapor diffusion method. Crystals grew to more than 0.1 mm length and it was a suitable size for X-ray data collection. The crystal is showed in **Fig. 5** (b).
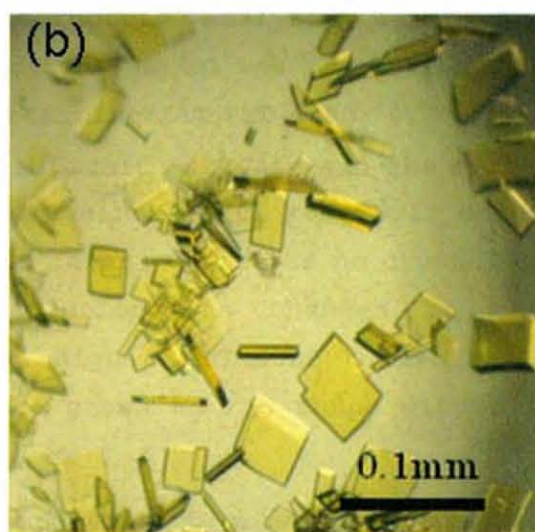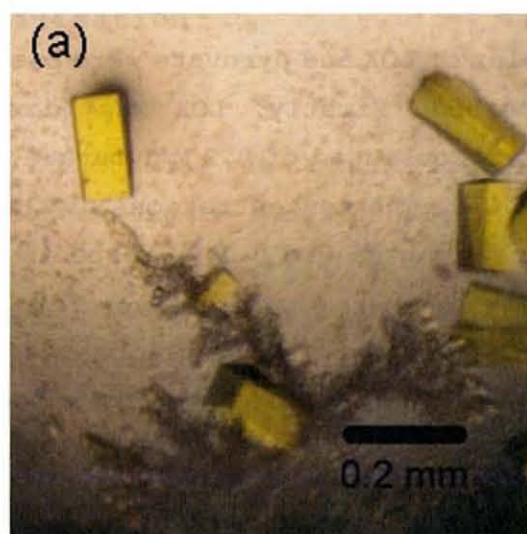
Fig. 5 (a) Native LOX crystal and (b) LOX-pyruvate complex crystal

2.4 X-ray data collection

The crystals were soaked for approximately 20-30 sec in a cryo-protectant solution which contains 10-20 % Glycerol in the reservoir solution prior to X-ray diffraction experiment at synchrotron facilities. In the case of LOX-pyruvate complex crystal, the cryo-protectant solution contained 0.1 M pyruvate.

The crystal was mounted in a cryo-loop and flash-cooled in a nitrogen gas stream at 100 K. The Diffraction data of native LOX crystal were collected at beamline BL38B1, SPring-8 and LOX-pyruvate complex was collected at NW12, Photon factory in KEK. Both beamlines were equipped with a CCD detector. The detail of the measurement parameters are listed in **Table 2**.

All images were processed by *HKL2000* program package (Otwinowski & Minor, 1997). The summary of both data collection were presented in **Table 3**. Native LOX crystal belongs to the tetragonal space group *I*422. Assuming four LOX molecules with a molecular weight of 41 kDa were in an asymmetric unit and thus 64 monomers in the unit cell, Mathews coefficient (V_M) was 2.71 $\text{Å}^3\text{Da}^{-1}$ which was in the normal range for the globular protein, and was equivalent to a solvent content of 54.6%. On the other hand, LOX-pyruvate complex crystal is monoclinic space group *C*2. There were four monomers in an asymmetric unit and 16 monomers in unit cell, resulting in V_M of 2.2 $\text{Å}^3\text{Da}^{-1}$ and a solvent content of 44.6 %.

19

Table 2　The data collection parameters

	Native LOX	LOX-Pyruvate
Beam line	BL38B1(SPring-8)	NW12(KEK PF)
Wavelength (λ)	1.0	1.0
Detector	CCD(Jupiter 210)	CCD(Quantum 210)
Camera distance (mm)	205	180
Exposed time (sec)	20	4
Oscillation range (°)	1.0	0.5
No. of collected frame	180	360
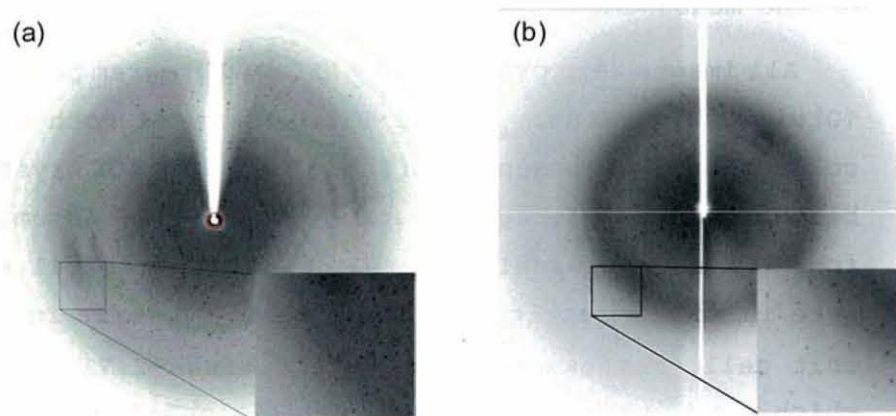
Fig. 6　The X-ray diffraction images, (a) Native LOX and (b) LOX-pyruvate complex

Table 3 crystal data and statistics of intensity data

	Native LOX	LOX-pyruvate
Space group	$I422$	$C2$
Unit cell		
a(Å)	191.10	134.84
b(Å)	191.10	118.57
c(Å)	194.50	107.24
α(°)	90	90
β(°)	90	121.07
γ(°)	90	90
Resolution (Å)	2.07 (2.14-2.07)[a]	1.9 (1.97-1.9)
Measured reflections	1,391,263	427,875
Unique reflections	108,566	113,367
Completeness (%)	100 (100)	99.5 (98.8)
Multiplicity	12.8 (10.5)	3.8 (3.6)
$I/\sigma(I)$	22.7 (4.52)	34.1 (5.3)
R_{merge}[b]	0.142 (0.436)	0.053 (0.226)
V_M /solvent content (%)	2.71 / 54.6	2.24 / 45.1

[a] Numbers in parentheses are for reflections in the highest resolution shell. [b] $R_{merge} = \Sigma | I_i - <I> | / \Sigma I_i$ where I_i are the observed intensity and $<I>$ is the average intensity of multiple observation of symmetry-related reflection.

2.5 Structure determination

Molecular replacement

The structure was determined by the molecular replacement method using *CNS* program. Glycolate oxidase (PDB code: 1GOX), which was a member of family and has 35.4 % sequence identity to LOX at the amino acid level, was used as an initial search model.

There could be four monomers in the asymmetric unit, because the V_M value was estimated to 2.71 $\mathring{A}^3$/Da calculated with the molecular weight of LOX (41 kDa) and its unit-cell volume (Matthews, B. W., 1968). A four-fold axis making tetrameric conformation was conserved in family enzymes. Furthermore, the previous report has shown that LOX forms a tetramer with non-crystallographic four-fold axis and such four-fold axis is inclined at 15 degree from *c*-axis in self-ration function analysis (Morimoto, Y., et al., 1998). Thus, we used a four-fold axis being a tetramer of GOX as the initial search model.

Four peaks related by four-fold symmetry were significantly higher than the others in the result of a cross-rotation function search (**Table 4-1**) which was calculated from the relationship between Patterson functions of the model structure and those of an unknown structure.

Then the tetramer model was located on a unique position in the crystallographic asymmetric unit by searching a translation function (**Table 4-2**). Because

the result indicated that higher four peaks related by four-fold axis were solved and no serious overlap was detected, a reasonable tetrameric structure was obtained and was used for the further structural refinement.

Table 4-1   Solutions of cross-rotation function search

	theta1 [a]	theta2	theta3	RF-function [b]
1	76.9	18.0	37.8	0.032
2	346.9	18.0	307.8	0.031
3	166.9	18.0	127.8	0.031
4	256.9	18.0	217.8	0.031
7	144.3	-3.5	150.8	0.021
8	157.9	19.2	118.8	0.019
9	247.9	19.2	208.8	0.018
10	337.9	19.2	298.8	0.018

a: Theta 1,2 and 3 are the Eulerian angles of rotation function search.

b: RF-factor is the index of the cross-rotation function searches.

Table 4-2 Solutions of translation function search

	Theta1	Theta2	theta3	transX	transY	transZ[a]	Monitor[b]	Packing[c]
1	69.4	18.8	45.6	-88.1	30.3	-107.5	0.29	0.487
2	339.4	18.8	315.6	-93.2	46.8	37.1	0.29	0.487
3	159.4	18.8	135.5	61.8	51.8	-124.3	0.28	0.487
4	249.3	18.8	225.7	-83.0	67.3	20.2	0.28	0.487
5	347.1	5.1	307.2	75.9	65.4	35.6	0.10	0.343
6	156.8	18.9	121.1	72.4	-71.7	30.9	0.09	0.267
7	247.7	19.0	208.5	95.8	28.4	45.0	0.09	0.339
8	335.6	19.2	300.9	-49.4	8.76	28.0	0.09	0.279
9	66.0	19.1	30.5	21.7	-1.9	-116.3	0.09	0.279
10	149.3	78.5	118.5	68.6	-79.8	32.7	0.07	0.440

a: Theta 1,2 and 3 are the Eulerian angles of rotation function search, and trans 1,2 and 3 are the vectors of translation function search.

b: Monitor values indicates the value of these searches.

c: The packing values consist of the ratio the molecular volume to the unit-cell volume.

25

2.6 Crystallographic refinement

R-factor and free R-factor

An R-factor (R_{work}), $\Sigma|F_o-F_c|/\Sigma|F_o|$, is used as refinement indicator, where F_o and F_c are an observed and a calculated structure factors, and summation is carried out for reflections.

A free R-factor (R_{free}) is calculated for the reflection that is not used for the refinement it stands for a reliability factor of structural refinement. It is calculated from a small fraction of reflections chosen at random before refinement begins and these reflections are eliminated from the refinement process. 5 % of reflection data was omitted from the refinement to monitor progress of the refinement as a free-R factor (Brünger, 1992). The free-R factor is an unbiased estimate of the improvement of the model.

All refinements were carried out using *REFMAC5* program in *CCP4* suite (Collaborative Computational Project, 1994) and *CNS* program package (Brunger, A. T., et al., 1998). When the refinement program was changed between *CNS* and *REFMAC5*, the test set was preserved.

Rigid-body refinement for calculating symmetry matrices

The structural model of tetramer determined with the GOX structure was replaced by the LOX sequence. Each position of the four molecules in the asymmetric unit and its non-crystallographic symmetry (NCS) matrices were optimized using rigid-body refinement. Thus, relative position and rotation angles among four monomers were refined.

Improvement geometry of LOX

Simulated annealing refinement using torsion angle dynamics was calculated with *CNS* program to reduce structural ambiguities. In its method, model structure was heated and cooled down slowly in virtual simulation. It decreases two factors; one is energy derived from conformational distortion and inter-molecular repulsion, and the other is the discrepancy between the observed and the calculated structure factors.

The structure was refined to consider the prevention of the steric clash and to preserve the non-covalent interaction within their proper values. And it was refined under structural restraint of the geometry of the main chain based on an ideal structure. The restraint includes their bond length, bond angle and the torsion angle of planar groups which are composed of atoms of the peptide linkage.

27

Model-building and improvement of density map

The structural model was revised in electron density maps using the graphic programs, *COOT* (Emsley, K., et al., 2004) and *XtalView* (McRee, D. E., 1993).

A composite-omit map which was affected less than other maps by the structure included in calculation of structure factors was composed for the structure revision. The composite-omit map is calculated in following method. Small regions (5 % of the model) of structure are systematically excluded and a small map covering the omitted region is calculated by the phase information from residual structure. Then, these small maps are formed as a continuous map. In addition to the composite-omit map F_o-F_c map was used to check the model error and find solvent molecules.

An outer loop, an amino-terminus and a carboxyl-terminus were not visible in the initial electron density map calculated with phases obtained by the molecular replacement method.

The electron density map was improved by using density modification methods, solvent flattening, histogram matching and NCS averaging method. The solvent flattening method set the electron density of solvent region to a mean value, 0, while the protein part of the map was unaltered. And a histogram matching method is applied to the protein region. The histogram computed from the electron density map of all protein regions is compared with histograms calculated from

ideal protein structure and the calculated histogram is fitted to an ideal histogram. NCS averaging method averaged the electron density of four molecules in asymmetric unit and the averaged density of the asymmetric unit was expanded to the unit cell.

The modified electron density was used to calculate to improve phase angles and they produce an improved map. Some unclear density map regions, flexible loop regions and terminal regions were improved by the density modification.

Refinement at the final stage

When the R_{free} value was decreased to below 30 % in the final stage of the structural refinement, the structure were inspected by using a difference Fourier map (F_o-F_c map) and solvent molecules were picked up from a F_o-F_c map. Since some parts of an enzyme molecule significantly deviated from the non-crystallographic four-fold symmetry of the tetramer, the NCS restrain weight was lowered gradually and finally excluded. The model geometry was analyzed with *PROCHECK* program (Laskowski, R. A., et al., 1993). The result was shown in **Fig. 9**.

The final coordinate have been deposited in the Protein Data Bank (PDB code: 2DU2). The final model and model quality statistics are presented in **Table 5**.

2.7 Structure determination of substrate analog and FMN

LOX-pyruvate complex structure was determined by the molecular replacement method using a tetramer of the native LOX as a search model. The refinement process was initially carried out under the NCS restraint of the tetramer. Since one of four molecules of the tetramer significantly deviated from an ideal four-fold model generated by the non-crystallographic symmetry, the NCS restraint was released in the final stage of the refinement. This is partly because one of four molecules lost electron density of the bound pyruvate, while the other three molecules have a clear electron density of the pyruvate molecule (**Fig. 7**).

The F_o-F_c map showed a clear electron density of a pyruvate molecule existing above si-face (**Fig. 8**) of the flavin-ring of FMN molecule, except one of four molecules where no electron density for the pyruvate molecule was observed. The pyruvate and FMN molecules were refined under geometrical restraints.

The flavin-ring was defined initially as a flat structure, but the electron density map appeared to bend slightly. For this reason, we released restraint of a flat structure of the central ring of the flavin-ring. Such restraint was defined as two-plane structure composed of a pyrimidine ring and a dimethylbenzene ring where border atoms (N5 and N10) between two rings were overlapped (**Fig. 8**). The flavin-ring was capable of

30

bending around N5-N10 axis because of the low geometry limitation. The structural models of flavin-ring were fitted to the map, which was calculated without the flavin molecules information, by real-space refinement using *COOT* program and the following structural refinement was calculated with this additional definition. The angle between two planes (dimethyl-ring and pyrimidine-ring) was defined as the dihedral angle of flavin-ring and it was calculated using the program *GEOMCALC* from *CCP4* suite. The dihedral angles of the two-ring of each monomer in the complex and the native LOX are shown in **Table** 6.

The composite-omit map showed that an isoalloxazine ring of a monomer that had no pyruvate molecule exhibited a flat structure, while those of the other three molecules containing a pyruvate molecule puckered at the central ring.
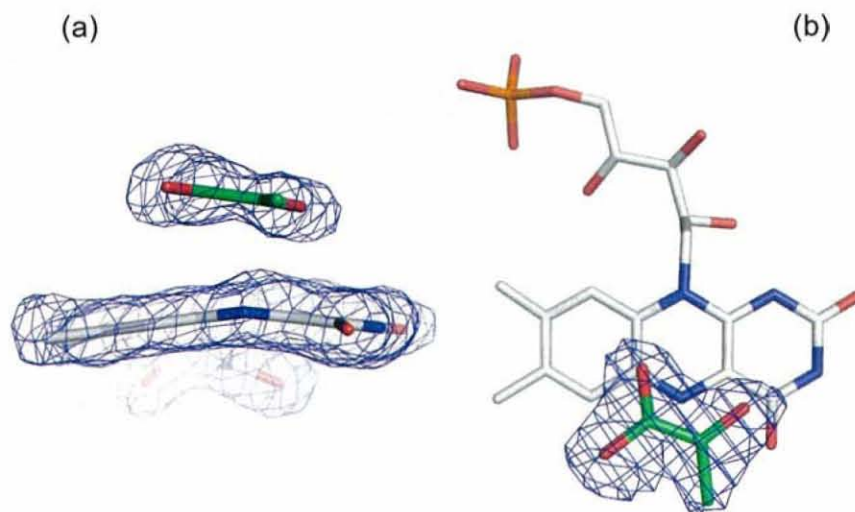
Fig. 7 F_o-F_c omitted difference map corresponding FMN and pyruvate molecules drawn at the 4 σ level: (a) The edge-on view from N5-atom side which shows the bent flavin-ring and (b) the view over the *si*-face of FMN. The electron density was calculated by omitting FMN and pyruvate molecule. Grey, blue and red colors of FMN are carbon, nitrogen and oxygen/phosphorus atoms, respectively, and green and red of the pyruvate are carbon and oxygen atoms, respectively. All of the bound pyruvate molecules are located in the similar position.
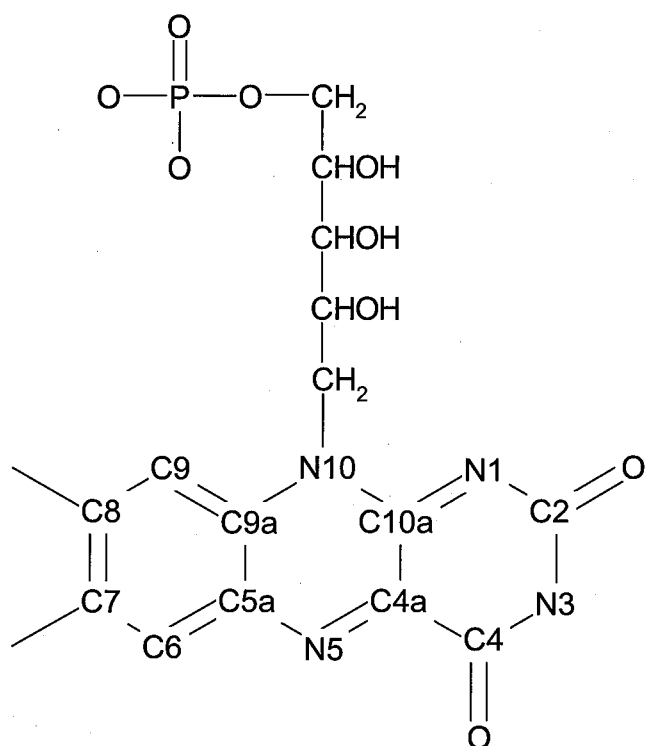
Fig. 8 The schematics diagram of FMN on the *si*-face. The figures show its chemical structures and its standard numbering of isoalloxazine ring atoms. Its left ring (C5a-C6-C7-C8-C9-C9a) is called dimethylbenzene ring and right ring (N10-N10a-N1-C2-N3-C4-C4a) is called pyrimidine ring. The isoalloxazine rings of LOX bent around N5-N10 axis.

Table 5 Refinement statistics

	Native LOX	LOX-pyruvate
Resolution (Å)	46.0-2.07	37.4-1.9
R_{work} [a]/ R_{free} [b]	16.23 / 19.98	17.7 / 22.7
No. of atoms		
Protein atoms	11,564	11,396 [c]
FMN atoms	124	124
Water molecules	1,110	1,476
Average B-factor (Å^2)		
Proteins	16.46	24.48
Water molecules	25.30	32.10
FMN / pyruvate	13.09 / -	20.25 / 30.13
$R.m.s.$ deviations		
Bond lengths (Å)	0.018	0.017
Bond angles (°)	1.782	1.665
Ramachandran plot [d]		
Most favored (%)	89.8	89.9
Allowed (%)	9.8	10.0
Disallowed (%)	0.4	0.2

[a] $R_{work} = \Sigma |F_o - F_c| / \Sigma |F_o|$ where F_o and F_c are the observed and calculated structure factor amplitudes, respectively. [b] R_{free} and R_{work} were calculated from the working set (95% of the data) and test set (5% of the data), respectively. [c] N-terminal residues (1-7) in each monomers were not determined. [d] Ramachandran plot were calculated using $PROCHECK$ program. (Laskowsk, R., et al., 1993)
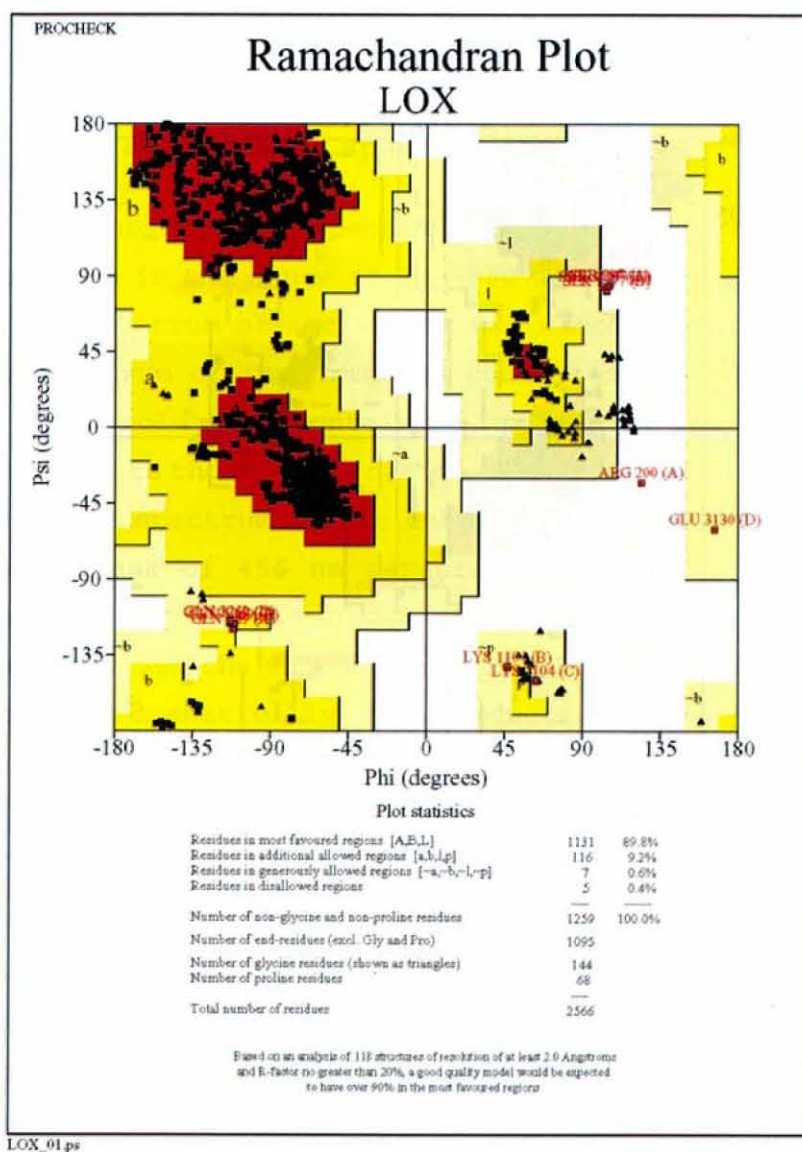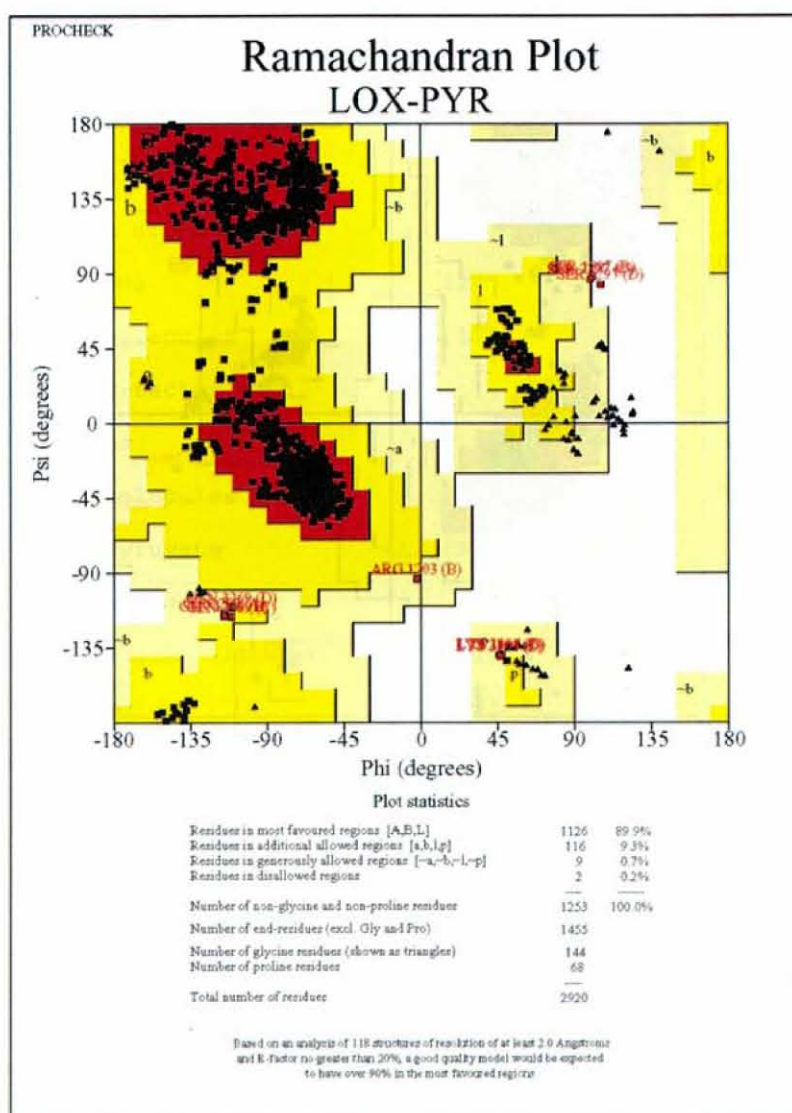
(a) **Native LOX structure**

Fig. 9 Ramachandran plots of the native LOX (a) and LOX-pyruvate complex (b). These figures were drawn by the *PROCHECK* program.

(b) LOX-pyruvate complex structure

PROCHECK

Ramachandran Plot
LOX-PYR

Plot statistics

Residues in most favoured regions [A,B,L]	1126	89.9%
Residues in additional allowed regions [a,b,l,p]	116	9.3%
Residues in generously allowed regions [~a,~b,~l,~p]	9	0.7%
Residues in disallowed regions	2	0.2%
	----	----
Number of non-glycine and non-proline residues	1253	100.0%
Number of end-residues (excl. Gly and Pro)	1455	
Number of glycine residues (shown as triangles)	144	
Number of proline residues	68	

Total number of residues	2920	

Based on an analysis of 118 structures of resolution of at least 2.0 Angstroms
and R-factor no greater than 20%, a good quality model would be expected
to have over 90% in the most favoured regions

LOX-PYR_01.ps

36

CHAPTER 3 : RESULT

3.1 The absorption spectrum analysis

The absorption spectra of four different LOX solutions in the range of 350-800 nm are given in **Fig. 4**. The spectrum of native LOX was almost identical to the spectrum of the oxidized condition. The spectrum of the solution containing pyruvate was almost identical to those of the native and the oxidized enzymes, while the spectrum of the enzyme reduced by L-lactate lost a peak of 456 nm detected for the others. The previous report has shown that the peak at 457 nm characterizes the enzyme-bound flavin structure and it decreases dramatically on the reduction (Maeda-Yorita, K., et al., 1995). The peak (456 nm) of spectrum of the LOX-pyruvate complex slightly shifted toward long-wavelength (red-shift) in comparison with those of the oxidized and the native enzymes.

From this report, the absorption spectra indicated that the FMN of LOX-pyruvate complex was the oxidized state than the reduced state. Therefore, LOX-pyruvate complex was not an enzyme-product complex (LOX_{red}-pyruvate) but a mimic structure of ES complex (LOX_{ox}-L-Lactate).

3.2 Structural features of LOX

Overview of monomer

Each monomer was composed of eight α-helices and eight β-sheets in a typical TIM barrel motif (Banner, D. W., et al. 1975). Eight helical structures were H1 (residues 104-115), H2 (128-136), H3 (151-164), H4 (224-234), H5 (246-254), H6 (276-287), H7 (302-310) and H8 (331-352), and eight β-strands were S1 (89-91), S2 (119-122), S3 (141-145), S4 (169-172), S5 (238-243), S6 (259-262), S7 (293-295) and S8 (315-318). An anti-parallel β-sheets, β1 (78-80) and β2 (83-85), were located at the bottom of the barrel like a lid-structure (**Fig. 10**).

A long-loop (172-224) which was inserted between S4 and H4 was located at the top of the barrel. This loop involved flexible segments with high temperature factors in low electron density region. The peptide chain for the poor region was built according to the electron density map improved by a density modification. This loop structure in the other family proteins has been not determined.

The FMN prosthetic group located at the carboxyl terminus of the β-barrel. The *si-face* isoalloxazine ring of FMN was exposed to the cavity and the ribityl side-chain of FMN molecule was buried inside barrel (**Fig. 10**).
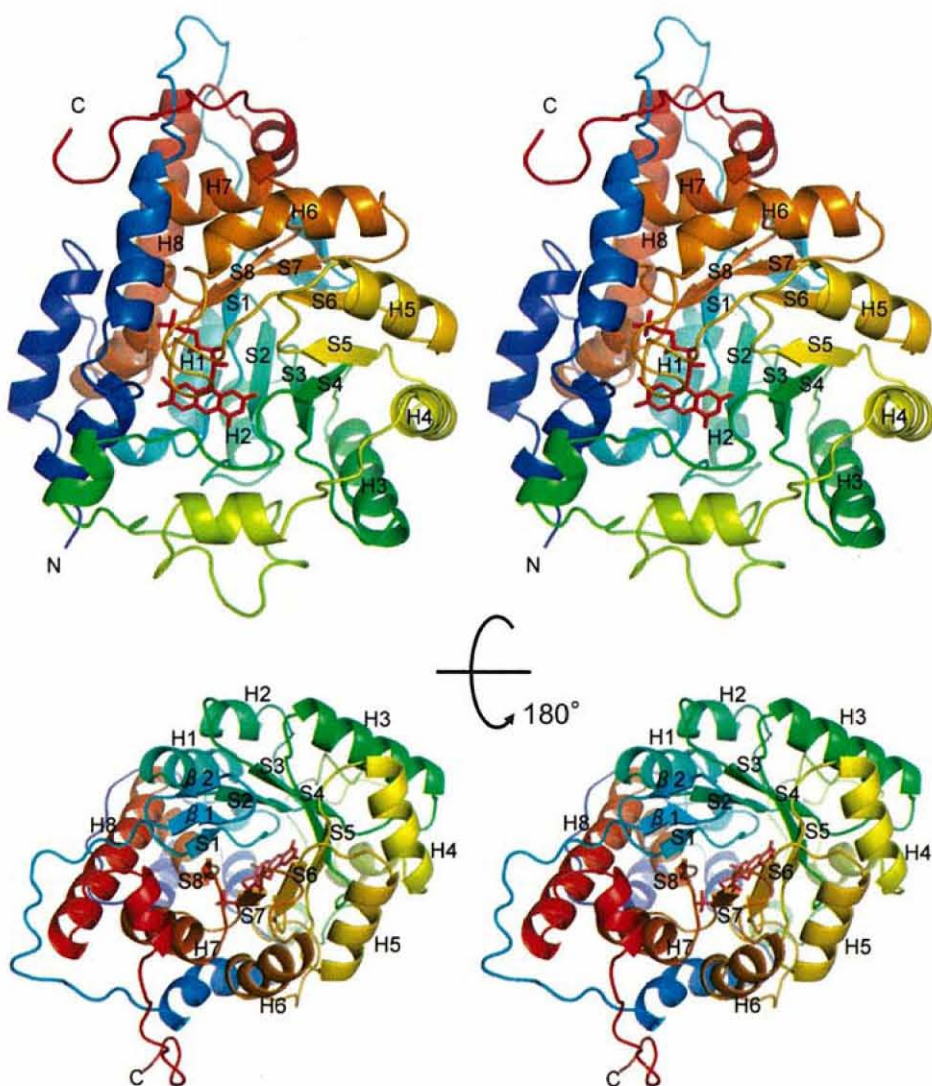
Fig. 10 Stereo view of the LOX structures. Each monomer exhibits a TIM barrel motif and the bottom of the barrel is closed by the anti-parallel β-sheets. FMN (red) is buried inside barrel.

Structural features of the cavity containing the active site

A cavity accessible to the active site exists at the C-terminal side of the β-strand barrel. The cavity is approximately 10 Å depth and its diameter is in the range of 4 ~ 10 Å. The entrance of the cavity is composed of two loop structures: loop LA (residue 181-191) and loop LB (212-215). It is shown in **Fig. 11**. These loops form the entrance concave of the cavity and they are fixed by two hydrogen bonds between Arg-181 and Tyr-215, and Tyr-191 and Asn-212. Loop LA includes small helix (182-187) and it is parallel up to the nearby helix (35-42). The conformation of loop LA is more stable than loop LB.

The cavity region is positively charged by the residues (lys-186, Lys-188 and Arg-181). These residues exist at the side of loop LA and two arginine residues (Arg-181 and Arg-268) are located at the end of the cavity. On the other hand, there is no charged residue in loop LB.
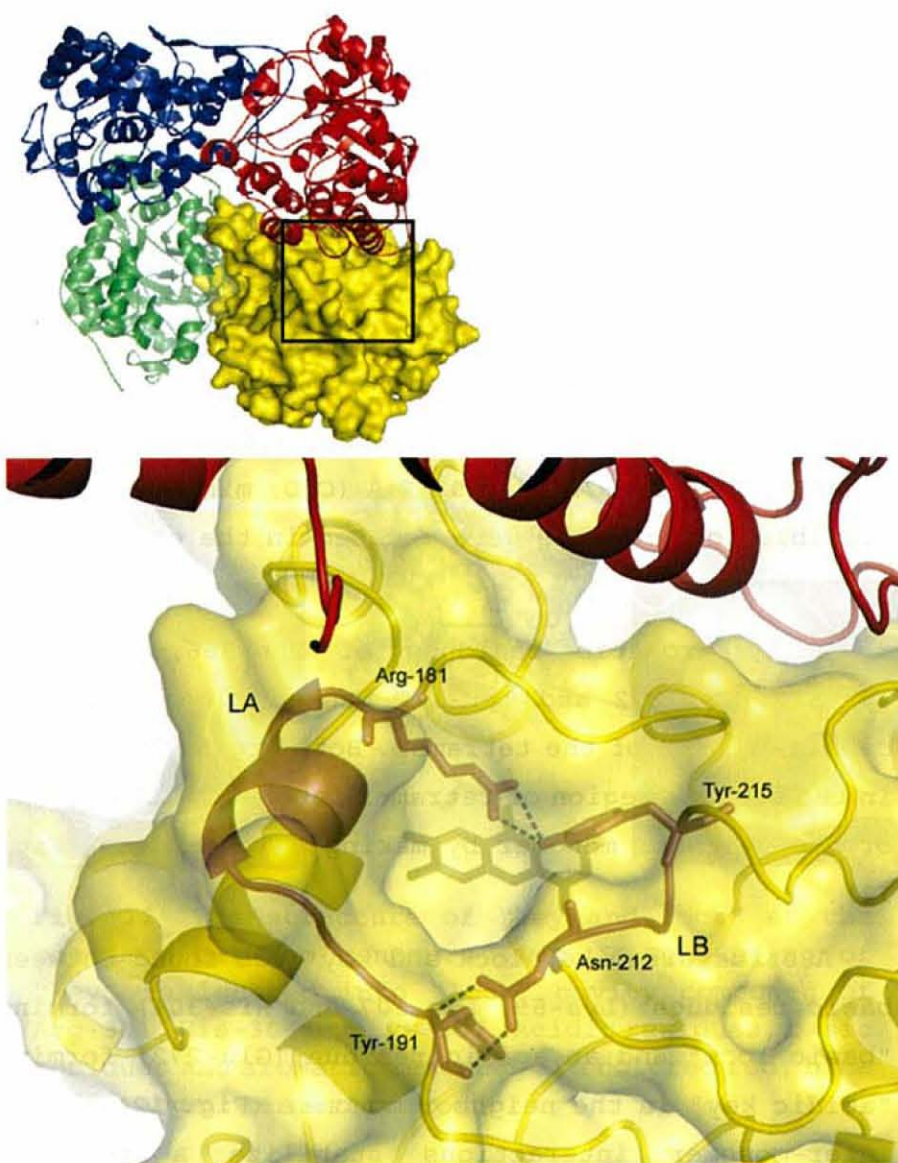
Fig. 11   The entrance of the cavity into the active
site is located at the corner of LOX tetramer. The
entrance (magentas) is between the loop segment (LA)
and the loop segment (LB). LA and LB are linked by
hydrogen bonds.

41

Tetramer structure

Both LOXs of the native and the LOX-pyruvate complex formed a tetramer with a four-fold symmetry. The C-termini of four monomers were in the central region of the tetramer. The *r.m.s.* deviations of Cα atoms among the four monomers of the native enzyme, excluding the N-terminal and the C-terminal regions (residues 1-21, 363-374) and flexible regions (173-225, 263-275), were 0.70 Å (A/B; maximum), 0.62 Å (A/C), 0.64 Å (A/D), 0.45 Å (B/C), 0.51 Å (B/D) and 0.42 Å (C/D; minimum). These flexible loop regions were located in the each corner of tetramer.

Bulky aromatic residues of Phe-366, Pro-369, Tyr-370, Tyr-372 and Tyr-374 packed closely in the central region of the tetramer. Both Arg-52 and Arg-56 in the central region of tetramer interact with Glu-373 of the neighbor monomer by making salt-bridges (**Fig. 12**).

A structure like "lock and key" was found between basic residues (Lys-59, Lys-307 and His-304) forming "basic lock" and an acidic residue (Glu-272) forming "acidic key" in the neighbor monomer (**Fig. 12**). These inter-monomer interactions stabilize a tetramer structure.
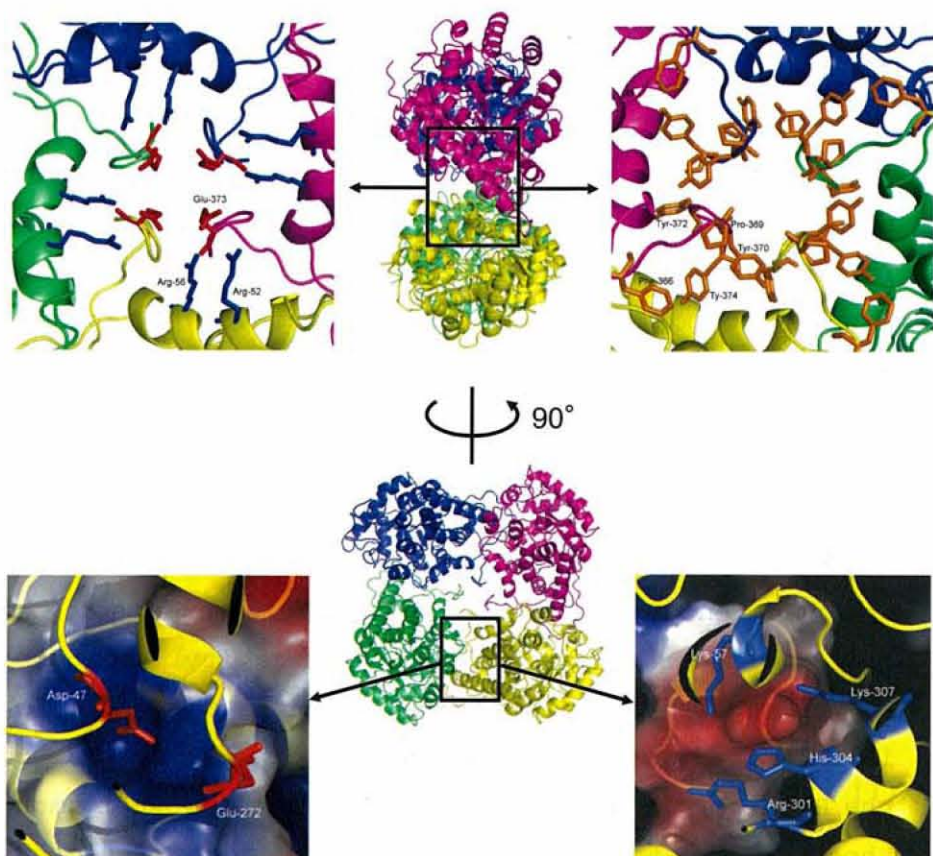
Fig. 12 The structure of "key and lock" at the boundary between monomers. Asp-47 consisting of "key" is located into "lock" cavity composed of Arg-301, His-304 and Lys-307. Acidic residues, basic residues and aromatic residues are colored red, blue and orange, respectively.

3.3 Structural comparison with other family enzymes

The structures of three family enzymes (FB2, GOX and LCHAO) have been determined by X-ray crystallography. Their sequence identities are less than 30 %, but they have the common structural motif and conserved residues at active site.

Comparison of tetramer assembly

The four-fold axis tetramer structure is conserved in family enzymes. The C-terminal region exists at the center of tetramer and the entrance cavity is exposed at the edge of tetramer. The C-terminal region of LOX is relatively stable compared with other enzymes, and the B-factor of this segment of LOX is the lowest among those of the family enzymes. The averaged B-factors calculated for five C-terminal residues are 14.3 Å^2 (LOX), 66.2 Å^2 (FB2), 41.1 Å^2 (LCHAO) and 37.4 Å^2 (GOX). The structural differences of four tetramers are shown in **Fig. 13**.
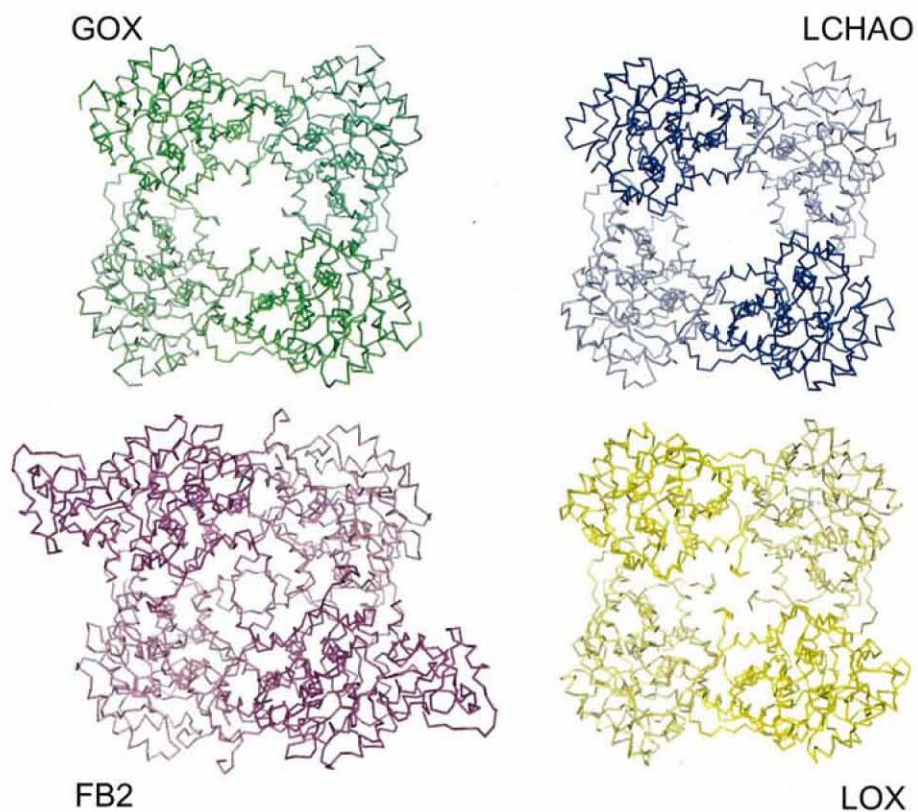
GOX

LCHAO

FB2

LOX

Fig. 13 The tetramer structure of family enzymes: LOX (yellow), GOX (green), LCHAO (blue) and FB2 (magenta). FB2 has been determined as a dimmer structure, but one of dimmer have not been determined in the N-terminal heme domain region.

Comparison of monomer structure

The α8/β8 barrel (TIM barrel) as a core-structure is strongly conserved (**Fig. 14**). The dimension of the barrel and each location of secondary structures are almost identical among these proteins, while they are different from each other in structures of both C- and N-terminal regions and the surface loop.

At the N-terminal region, the length of this segment of LOX is approximately 15 Å longer than those of GOX and LCHAO. That of FB2 is the largest among these enzymes and it includes a heme domain consisting of a protoporphyrin molecule. On the other hand, the C-terminal segment of LOX is also longer than GOX and LCHAO (GOX-LOX; about 19 Å longer than GOX, LCHAO-LOX; about 26 Å longer than LCHAO) and shorter than FB2 (FB2-LOX; about 91 Å shorter than FB2).

The surface long-loop structure (residues 174-224) which is a joint between fourth sheet (S4) and fourth helix (H4) in TIM barrel is different among family enzymes in their conformations and sequences. The corresponding regions of other family enzymes (residue 299-317 in FB2, 188-202 in LCHAO and 188-198 in GOX) had not been determined. The portion (206-216) of this loop structure in LOX covered the hole of the active site, while corresponding loops of the other enzymes were away from the active site (**Fig. 15**).
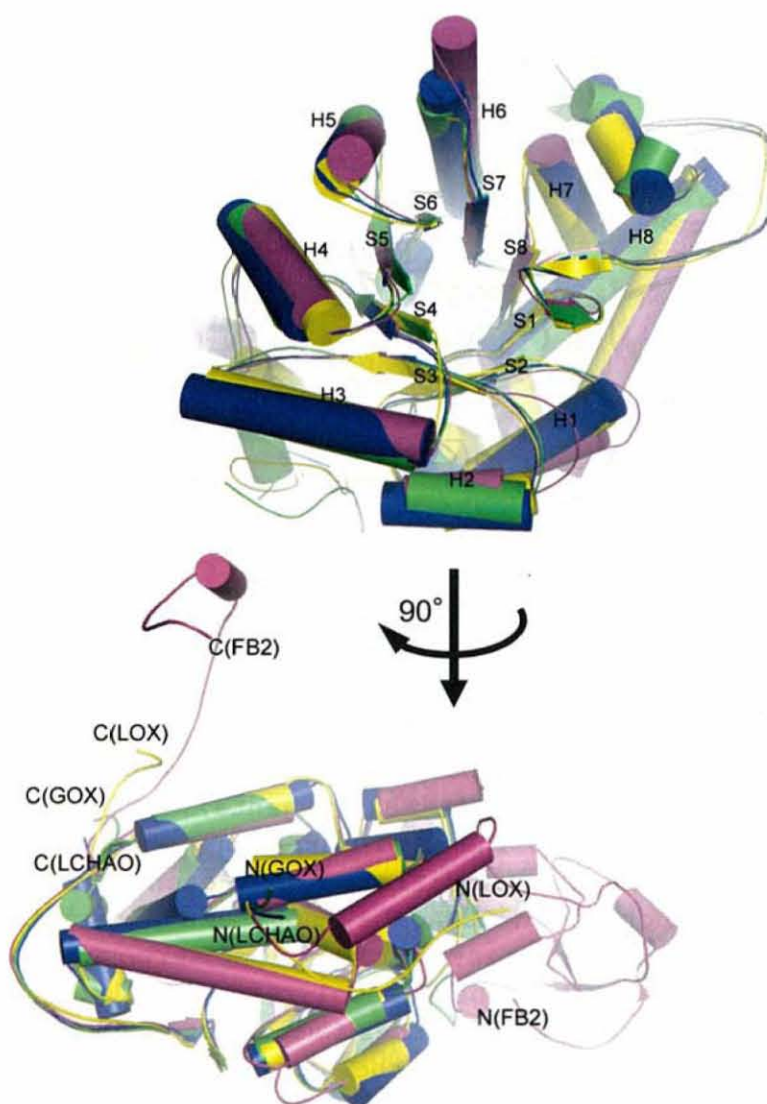
46

Fig. 14 TIM barrel structure is conserved in family enzymes; LOX (yellow), FB2 (magenta), GOX (green) and LCHAO (blue). Each eight helices (H1-H8) and eight sheets (S1-S8) were located in similar positions respectively. However, the terminal structures are different from each other. N-terminus of FB2 composes a heme domain.
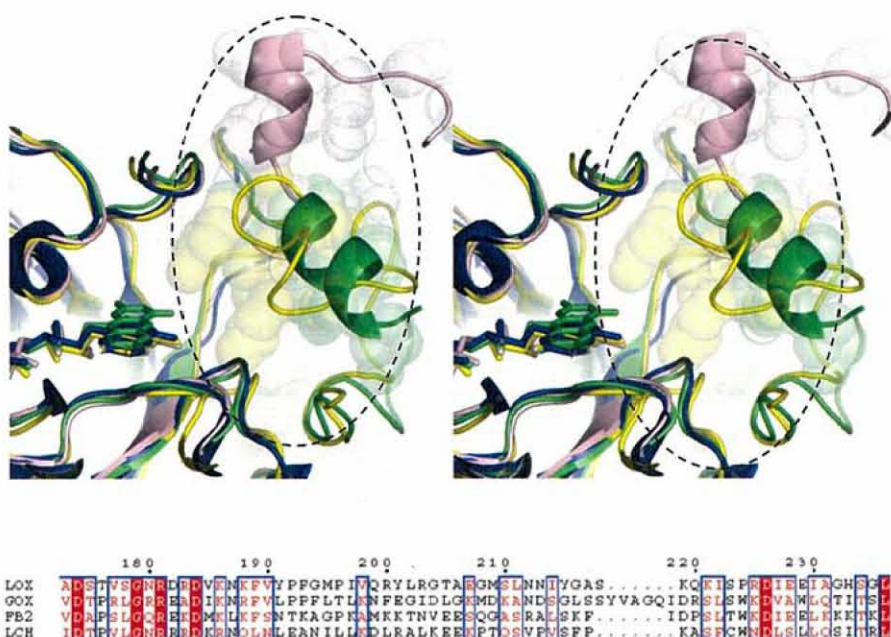
```
              180         190         200         210              220          230
LOX   ADSTVSGNRLRDVKNKFVYPFGMPIVQRYLRGTARGMSLNNIYGAS......KQKISFRDIEEIAGHSGL
GOX   VDTFRLGRRERDIKNRFVLPPFLTLKNFEGIDLGKMDKANDSGLSSYVAGQIDRSLSWKDVAWLQTITSL
FB2   VDAPSLGQRERDMKLKFSNTKAGPKAMKKTNVEESQGASRALSKF......IDPSLTWKDIEELKKTKL
LCH   IDTPVLGNRRRDKRNQLNLEANILLKDLRALKEEIPTQSVPVSFP.......KASFCWNDLSLLQSITRL
```

Fig. 15 Stereo view of the long loop region (dotted circle) in the superposed model among family enzymes; LOX (yellow), FB2 (magenta), GOX (green) and LCHAO (blue). The each long-loop, which covers their active site, is different from each other. The loop structure in LCHAO has not been determined. These residues consisting of the loop structures are represented with sphere-model respectively. Their loop structures in the other family enzymes (GOX and FB2) do not rigidly cover the active site in contrast to LOX. The bellow multi-sequence alignment of LOX with other families corresponds to the long loop region (LOX: residue 174-224).

48

Comparison of active site structures

Most of residues at the active site are highly conserved in family enzymes (**Fig. 16**). The orientations of FMN in the protein molecules were compared by superposing with amino acid residues of the active site. The FMN molecules were superposed well among those of the family enzyme except for the flavin-ring of GOX.

The some residues at the *si*-face of flavin-ring were not conserved. Tyr-40 of LOX was replaced by Phenylalanine in LCHAO and Tyr-124 of LOX was replaced by Leu-230 in FB2, Trp-108 in GOX and Tyr-107 in LCHAO. Leu-230 of FB2 was located between a protoporphyrin molecule and FMN molecule, alternatively this position in other enzymes was occupied by a bulky aromatic residue, tyrosine or tryptophan. (**Fig. 16**)

The segment of the long-loop structure (174-224) rigidly covered the active site (**Fig. 15**), but these residues in two enzymes (FB2 and GOX) are loosely covered and this region structure of the LCHAO is not known. This segment which is composed of some bulky hydrophobic residues (Tyr-215 and Leu-211), but in other enzymes, small hydrophobic residues are located in this region (Leu-286 in FB2 and Leu-161 in GOX) and the loop structures are away from their active site in contrast to LOX. Their active site cavities are expanded up, but the cavity of LOX is rigidly closed by loop structure.
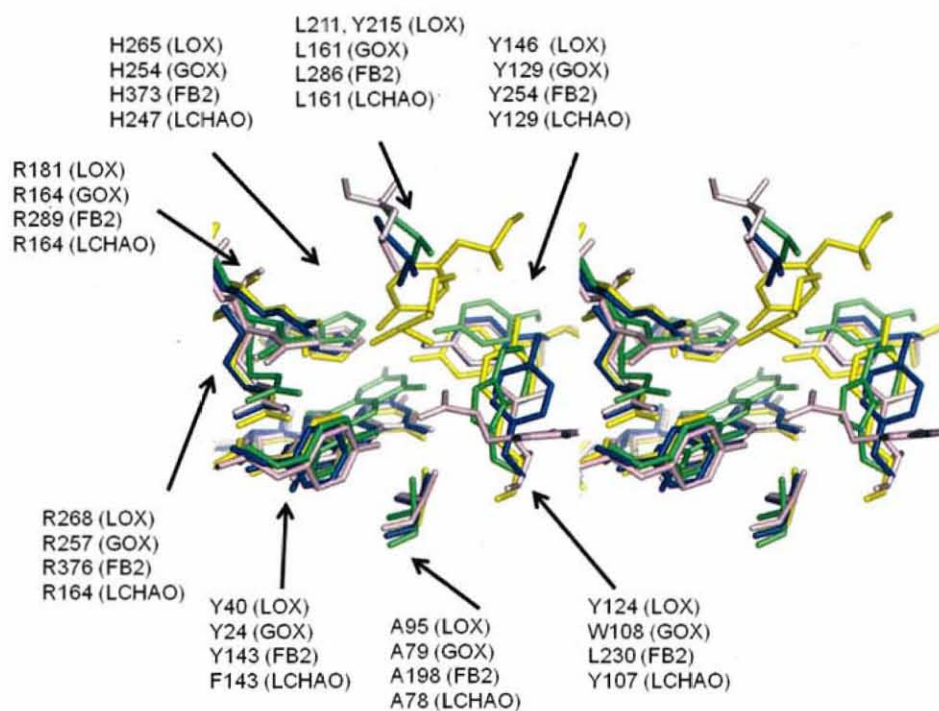
H265 (LOX)
H254 (GOX)
H373 (FB2)
H247 (LCHAO)

L211, Y215 (LOX)
L161 (GOX)
L286 (FB2)
L161 (LCHAO)

Y146 (LOX)
Y129 (GOX)
Y254 (FB2)
Y129 (LCHAO)

R181 (LOX)
R164 (GOX)
R289 (FB2)
R164 (LCHAO)

R268 (LOX)
R257 (GOX)
R376 (FB2)
R164 (LCHAO)

Y40 (LOX)
Y24 (GOX)
Y143 (FB2)
F143 (LCHAO)

A95 (LOX)
A79 (GOX)
A198 (FB2)
A78 (LCHAO)

Y124 (LOX)
W108 (GOX)
L230 (FB2)
Y107 (LCHAO)

Fig. 16-1 Stereo view of superposed active site residues conserved in family enzymes: LOX (yellow), GOX (green), FB2 (magenta) and LCHAO (blue).
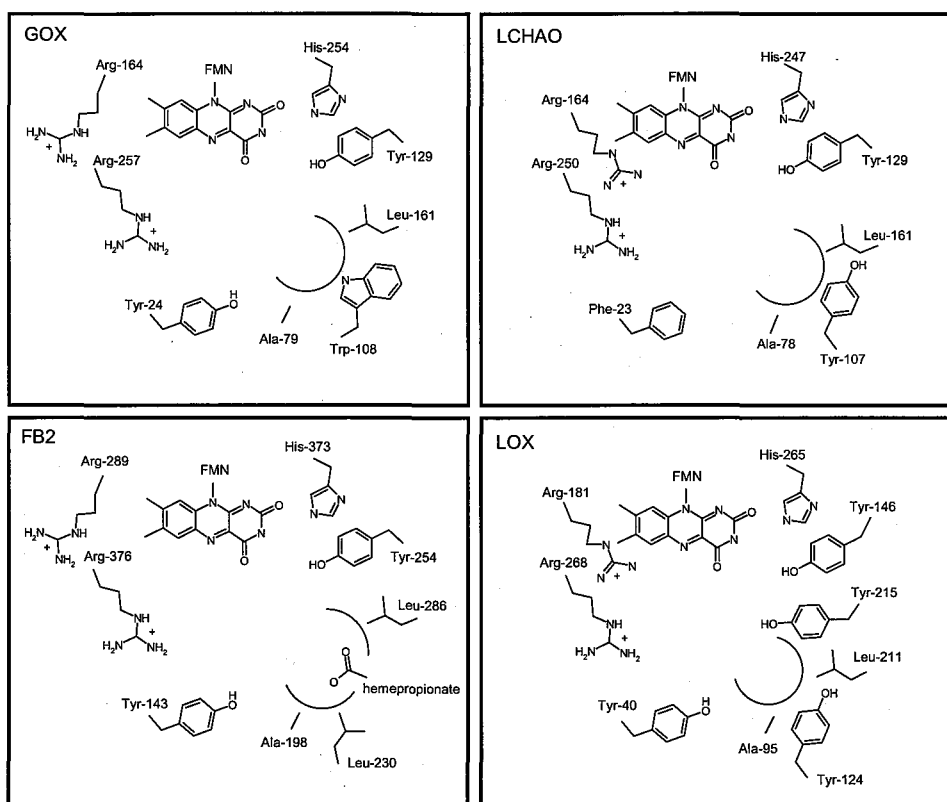
Fig. 16-2 Schematic representation of the active site resides in LOX and family enzymes. Arg-181, Arg-268, His-265 and Tyr-146 in LOX are strongly conserved in family enzymes. but, Tyr-40 in LOX is changed to Phe-23 in LCHAO, and Tyr-124 in LOX is changed to Trp-108 in GOX and Leu-230 in FB2. The semicircle represents the hydrophobic pockets, whose components are different from each other.

3.4 Overview of LOX-pyruvate complex

The LOX-pyruvate complex structure (**Fig. 17**) was used for the model structure of the enzyme-substrate complex in order to gain insight into the catalytic mechanism. The catalytic reaction of LOX was elucidated by inspecting the structural model of ES complex.
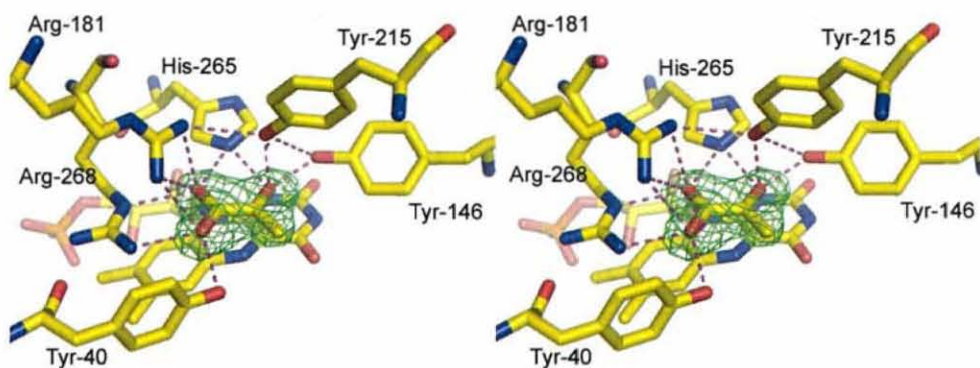

Fig. 17 The bound pyruvate located near the active site. The mesh (green) indicates F_o-F_c omitted map (at 4 σ level) corresponding to the bound pyruvate. Dotted lines (magenta) indicate the electrostatic interactions between the bound pyruvate and the active site residues in LOX.

3.5 Structural feature of LOX-pyruvate complex

The structure of LOX-pyruvate complex was determined at 1.9 Å resolution. The electron density of a pyruvate molecule is observed near the cofactor, FMN molecule in the complex crystal (**Fig. 17, Fig. 21**). The electron densities of the N-terminal region (residues 1-10) of the LOX-pyruvate complex was so low that we could not build peptide structure, but the map of the long-loop region (residue 195-215) was clearer than that of the native crystal. The large conformational difference of residues around the active site was not observed between the complex and the native structures (**Fig. 18**). Superposing the native enzyme and the LOX-pyruvate complex, *r.m.s.* deviation of Cα atoms of residues 10-374 was calculated. Their averaged value is 0.24 Å (SD 0.02) excluding one monomer from the calculation which did not hold a pyruvate.
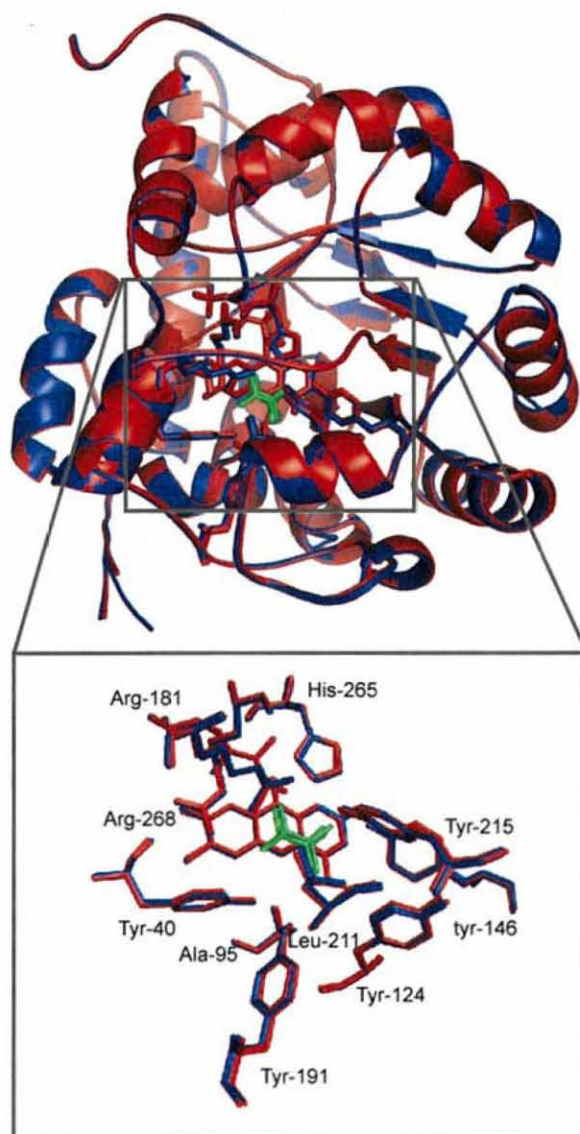
Fig. 18 The superposition of four monomers of the native structures (blue) and three monomers of the complex (red) except the non-liganded monomer. The bound pyruvate (green) of three monomers were located in the similar position.

The isoalloxazine ring of the complex curved along its long-axis and the central ring puckered about N5-N10 axis to close *si*-face of its plane-surface (**Fig. 19**). The distortion of this ring has been termed "butterfly bending" (Lennon, B. W., et al., 1999; Moustafa, I. M., et al., 2006) to indicate a rigid motion of the two end rings. The dihedral angles between the two planes (dimethyl-ring and pyrimidine-ring) of each monomer in the complex and the native LOX are shown in **Table 6**. FMN molecules of the LOX-pyruvate complex and native LOX were superposed within *r.m.s.* deviation of 0.1 Å. The flavin-ring of the complex crystal bent at an angle of average 4.2 degree more than those of the native crystal.
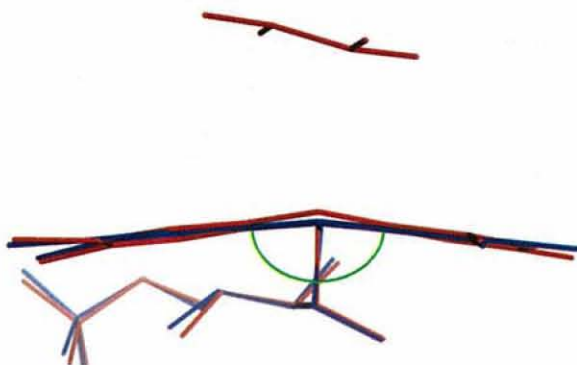
Fig. 19 The edge-on view of FMNs from N5-atom side was superposed. The FMN and pyruvate of the complex and the FMN of native are colored in red and blue, respectively. The measured dihedral angle is colored in green.

**Table 6 Dihedral angles of flavin-rings**

Native		NL			Average (°)
	169.1	169.3	169.8	168.5	169.2
Complex	ND	L	L	L	
	166.4	165.2	165.5	164.2	165.0*

*the value was averaged from the data of three liganded monomers. NL: non-liganded, ND: not detected, L: liganded

Crystal packing arrangement

The native LOX was crystallized in *I*422 space-group, while the crystal of the complex belonged to *C*2 space-group. Tetramer structure with a four-fold symmetry was conserved between the native and the complex crystals. The octamer arrangement, which was generated of tetramer with crystallographic symmetry, was not conserved (**Fig 20**). It did not suggest that the octamer in the native crystal was a physiological assembly. Two tetramers of octamer in the native LOX was piled up, while the tetramer in the complex slid off the head-on location. Therefore, each tetramer in the complex is piled up parallel. In contrast, the octamer in native LOX structure formed a four-fold assembly.

(a) Native LOX in *I*422 crystal
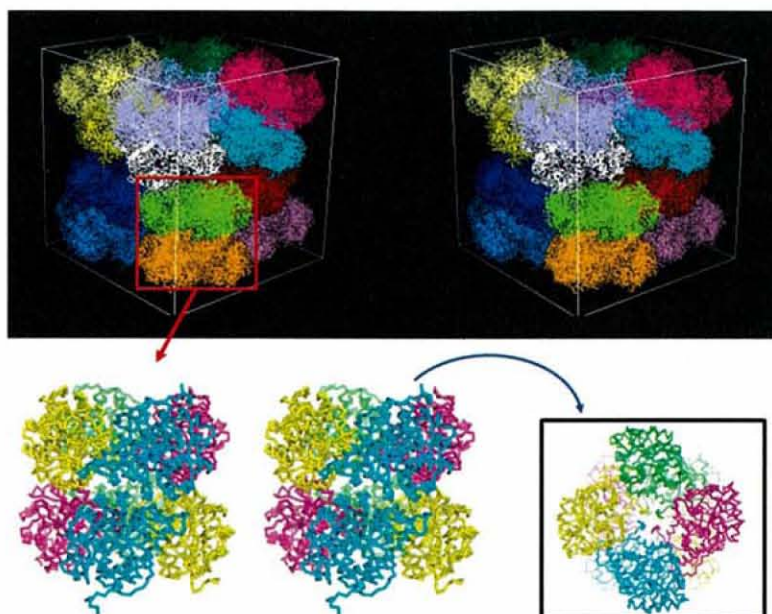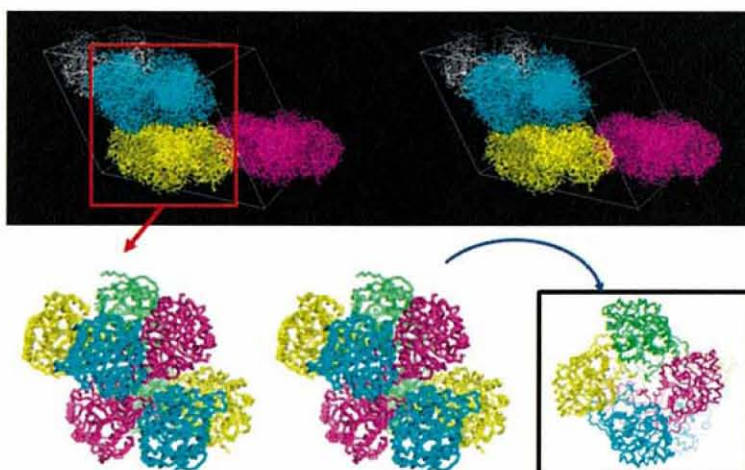

(b) LOX-pyruvate complex in *C*2 crystal

Fig 20 Crystal packing arrangement of LOXs in unit-cells and octamer arrangement. The top-view of octamer shows that arrangement of tetramer is conserved between native and complex.

57

3.6 Structure of the bound pyruvate molecule

The electron density peaks to correspond to pyruvate were observed in three monomers except one monomer (**Fig. 21**). The electron density peaks corresponding to the oxygen atoms of both the carboxyl group (-COO) and carbonyl group (-Cα=O) were unambiguously assigned. Thus, the orientation of the bound pyruvate was correctly determined.

In the native structure, the position of the bound pyruvate was occupied by two water molecules. The inter-atomic distances between atoms of pyruvate and those of residues interacting with the pyruvate molecule are shown in **Table 7**. The two oxygen atoms of carboxyl group were held with ionic interactions with Arg-181 and Arg-268. The carbonyl oxygen atom had hydrogen bonds with Tyr-215 and Tyr-146. The distance between N5 atom of FMN molecule and the C2 atom of pyruvate was average 2.9 Å which was significantly shorter than the sum of van der Waals radii of a nitrogen and a carbon atoms.
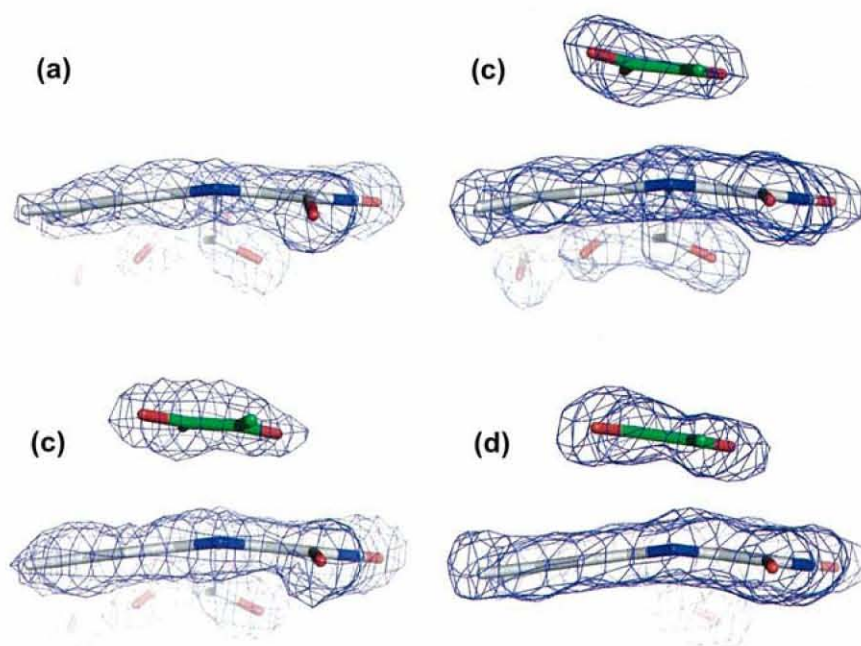
Fig. 21 The F_o-F_c omitted difference maps (4 σ level) of FMN and the bound pyruvate in each four monomers. A pyruvate molecule was observed in the maps of three monomers out of four (b, c and d), but it is not identified in the map of one monomer (a).

Table 7   The distances between a pyruvate and surrounding residues

Distance (Å)	Liganded three monomers			Average (SD)
Arg181– PYR				
N1 – O1	3.2	3.0	2.9	3.0 (0.16)
N2 – O2	2.8	2.8	3.1	2.9 (0.14)
Arg268 – PYR				
NE – O1	2.8	2.8	2.9	2.8 (0.08)
N1 – O2	2.7	2.7	2.9	2.8 (0.09)
Tyr40 – PYR				
O – O2	2.5	2.5	2.8	2.6 (0.16)
His265 – PYR				
NE2 – O1	2.9	2.7	2.6	2.7 (0.13)
Tyr215 – PYR				
O – O3	2.5	2.3	2.2	2.3 (0.22)
Tyr146 – PYR				
O – O3	2.5	2.6	2.4	2.5 (0.14)
FMN – PYR				
N5 – C2	2.7	3.0	3.0	2.9 (0.14)

PYR: pyruvate, SD: standard deviation
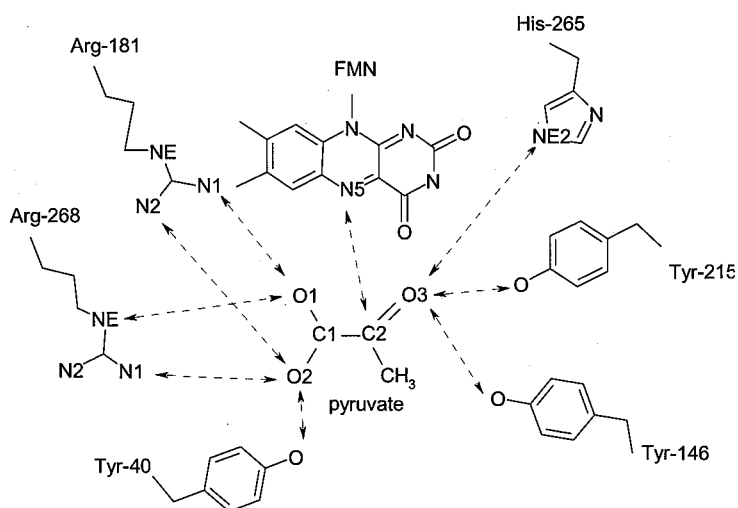
3.7 Inter-atomic interaction of the bound pyruvate and LOX

The pyruvate molecule was located at the *si*-face of the flavin-ring. Three different kinds of interactions between some active site residues and the pyruvate were observed: 1) Ionic interactions with carboxyl-group of the pyruvate, 2) hydrophobic interactions with its methyl-group and 3) hydrogen bond interactions of its carbonyl group (**Fig. 22**).
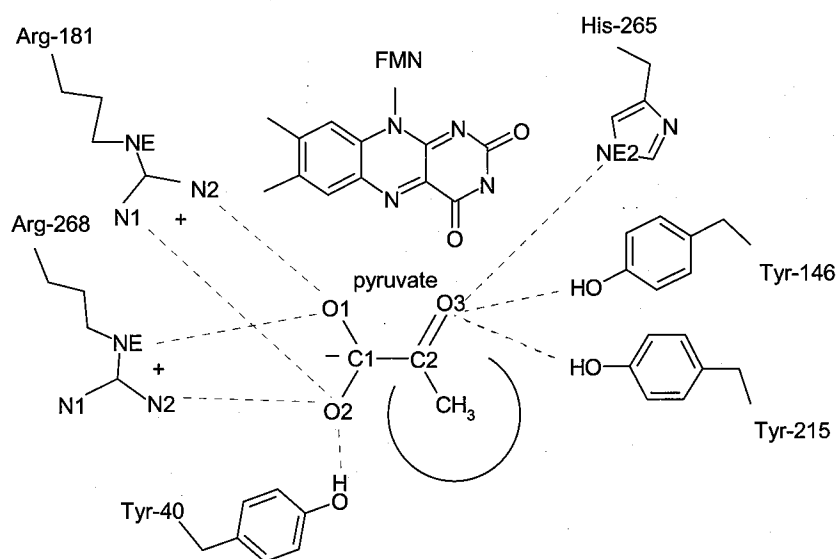

Fig. 22 Schematic diagram of the active site residues around the pyruvate. Ionic interactions (red) and hydrogen bonds (blue) are shown by dotted lines. The hydrophobic interaction is shown by semicircle.

1) *Ionic interaction*: The carboxyl group was joined in two ionic interactions with guanidinium side-chain (N2 and NE) of Arg-268 and guanidinium side-chain (N1 and N2) of Arg-181. The distances between cationic residues, Arg-181 and Arg-268, and anionic parts of pyruvate, carboxyl-group, are average 3.0 Å and 2.8 Å respectively.

2) *Hydrophobic interaction*: The methyl group of pyruvate was fitted well in the hydrophobic-pocket of the enzyme (**Fig. 23**) that consisted of two small hydrophobic residues (Leu-211 and Ala-95) and four aromatic residues (Tyr-146, Tyr-124, Tyr-215 and Tyr-191). The methyl-group of pyruvate closely contacted with Leu-211 from upper-side and Ala-95 from lower-side and was surrounded by four tyrosine-ring structures.

3) *Hydrogen bond interaction:* The oxygen atom (O2) of the group also was in the range of hydrogen bond with hydroxyl group of Tyr-40. The oxygen atom (O3) was also in range of hydrogen bond with two tyrosine residues, Tyr-146 and Tyr-215 (**Table 7**). These electrostatic interactions and hydrogen bonds fixed the pyruvate in the enzyme molecule.

The oxygen atom (O3) of the carbonyl group of the pyruvate faced toward the NE2 atom of histidine residue (His-265). The average distance between NE2 atom of His-265 and O3 atom of pyruvate was 2.7 Å (SD 0.12 Å).His-265 residue is important for the catalytic base, because the H265Q mutant in LOX showed that its enzyme

activity is almost abolished (Yorita, K., et al., 2005).
This histidine residue are highly conserved in family
enzymes (FB2; B Gaume etal., 1995 and LMO; Geogel,D.A.,
et al., 1990) and the similar biochemical experiments
have been reported for other family enzymes (Fb2; Gondry
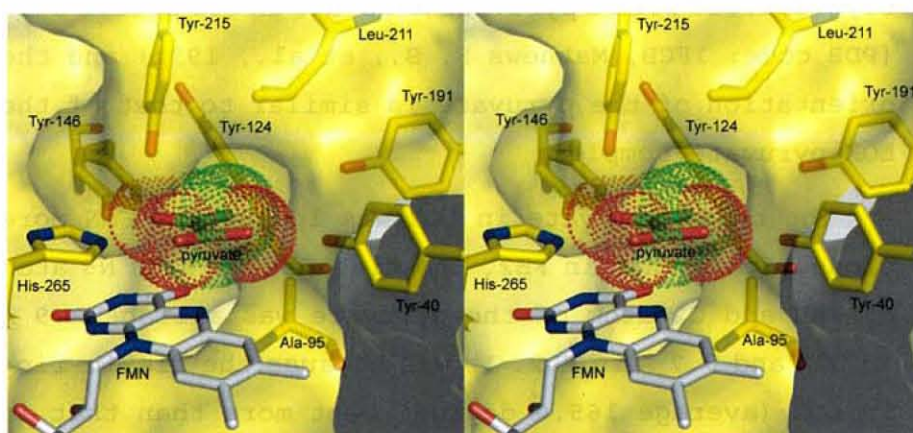M., et al., 1996 and LMO; Muh U., et al., 1994).

Fig. 23 The stereo view of the hydrophobic pocket.
The dotted spheres indicate the van der Waals radius.
Oxygen (red), nitrogen (blue) and carbon (yellow;
enzyme, green; pyruvate and gray; FMN) are colored,
respectively. The methyl group of pyruvate is
rigidly held in this pocket composed of Leu-211,
Ala-95 and five tyrosine residues. The oxygen atom
of the carbonyl group was located near His-265
residue.

3.8 Comparison with family enzyme involving a substrate

In general studies about the oxidation mechanism of α-hydroxy acid, FB2 structure has been frequently used. FB2 is well known in the family enzymes and it catalyzes oxidation of L-lactate as well as LOX. It has been crystallized with a pyruvate molecule in its active site (PDB code: 1FCB, Mathews F. S., et al., 1991) and the orientation of the pyruvate is similar to that of the LOX-pyruvate complex.

The bound pyruvate in LOX was located to FMN more closely than that in FB2. The distance between N5 atom of FMN and C2 atom of the pyruvate was average 2.9 Å in LOX and 3.7 Å in FB2. It was because the flavin-ring in LOX (average 165.0 degree) bent more than that in FB2 (173.1 degree).

The bound pyruvate in LOX was strongly fixed in the active site by two arginine residues (Arg-181 and Arg-268), three tyrosine residues (Tyr-40, Tyr-146 and Tyr-215), and the hydrophobic pocket consisting of Leu-211, Ala-95, Tyr-146, Tyr-124, Tyr-215 and Tyr-191.
On the other hand, the bound pyruvate in FB2 is fixed by one arginine residue (Arg-376) and two tyrosine residues (Tyr-143 and Tyr-256): the carboxyl group of pyruvate interacts with Arg-376 and Tyr-143, and its carbonyl group is hydrogen bonded with Tyr-256 (**Fig. 24**). The pyruvate in LOX interacts with its active site residues more strongly than that in FB2.

The methyl group in FB2 is loosely surrounded by small hydrophobic residues (Leu-230 and Leu-286). The rigid hydrophobic interaction of the methyl group is not found in other family enzymes (GOX and LCHAO). The hydrophobic pocket which is the characteristic of LOX has an important role for the enzyme to select an absolute configuration of a substrate as stated later.
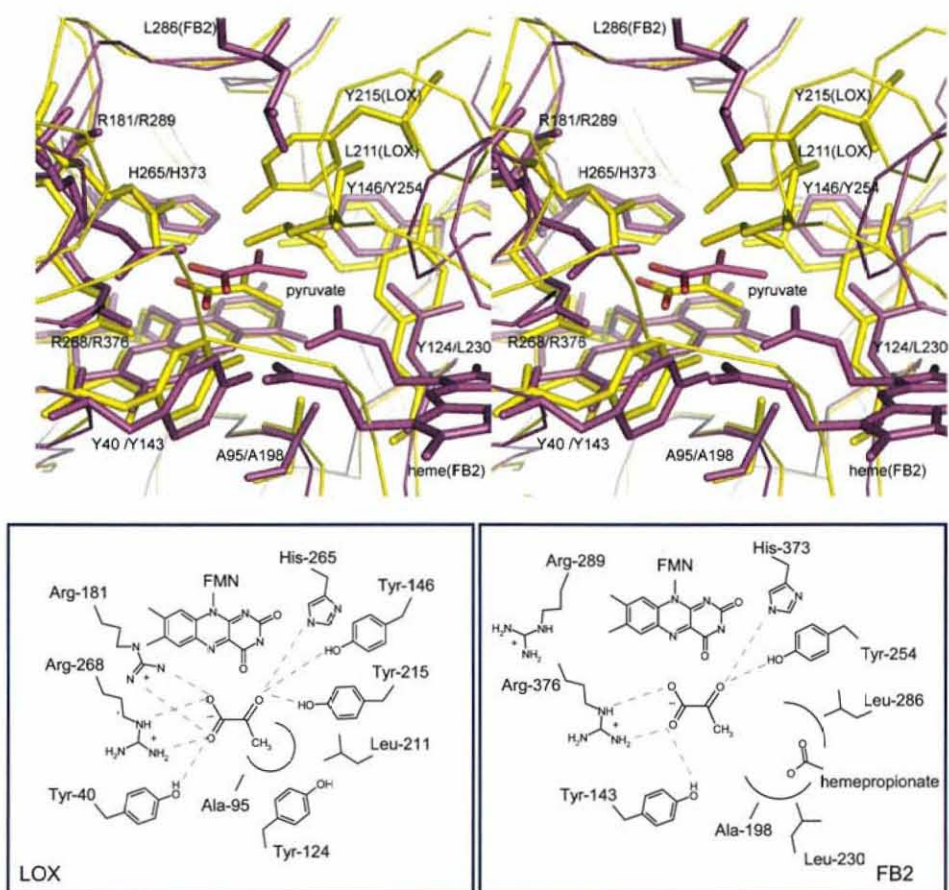
Fig. 24 Stereo view of the active site components in FB2 (magenta) and LOX (yellow) and their conserved residues are labeled (LOX/FB2), respectively. FB2 including a pyruvate are superposed to LOX. The schematics indicate the comparison of active site components of two enzymes.

3.9 The structural prediction of an ES complex

The model L-lactate was placed at the pyruvate site
by sharing the carboxyl group, the methyl group. The
model structure of LOX-lactate complex was refined to
be located in the geometrically reasonable position by
REFMAC5 program in structural idealization mode in *CCP4*
suite. The simulated structure is shown in **Fig. 27**.

The distances between the oxygen (O3) atom of the
hydroxyl-group of the model L-lactate and NE2 atom of
His-265 was about 3.0 Å (**Fig. 25**).

The distances between the oxygen atoms of two tyrosine
residues, Tyr-215 and Tyr-146, and the oxygen atom (O3)
of its hydroxyl-group were about 2.6 Å and 2.9 Å,
respectively. The hydrogen atom (HA) was located near
the flavin-ring and the distance between the hydrogen
atom (HA) and N5 atom of FMN was about 2.2 Å. Its
carboxyl-group was held with Arg-181 and Arg-268
residues with ionic interactions as well as the complex
with pyruvate.

D-lactate is the optical isomer of L-lactate, in
which the position of hydrogen atom (Cα-H) interchanges
to the position of hydroxyl group (Cα-OH). When the model
D-lactate based on the L-lactate conformation was placed
to the active site, its hydroxyl-group clashed with the
flavin-ring (**Fig. 26 (b)**).

A lactate molecule rotates freely around the C1-C2
axis and its substituents can be in the different

arrangements. When the model D-lactate molecule is twisted around C1-C2 axis outside the enzyme, it was possible to be located in active site cavity without steric hindrance (**Fig. 26 (a)**).

The twisted model D-lactate was refined as well as that of the non-twisted model L-lactate. The hydroxyl-group of the D-lactate was located near His-265 residue. The distance between the HB and the oxygen (O3) atom of its hydroxyl-group and the NE2 atom of His-265 was about 2.9 Å. But its hydrogen atom (HA) was far away from both His-265 residue and FMN. The distance between the hydrogen atom (HA) and chiral center atom (C2) of the model D-lactate and N5 atom of FMN is about 4.7 and 3.6 Å respectively. Its carboxyl-group was held with Arg-181 and Arg-268 residues with ionic interactions as well as the complex with the model L-lactate.
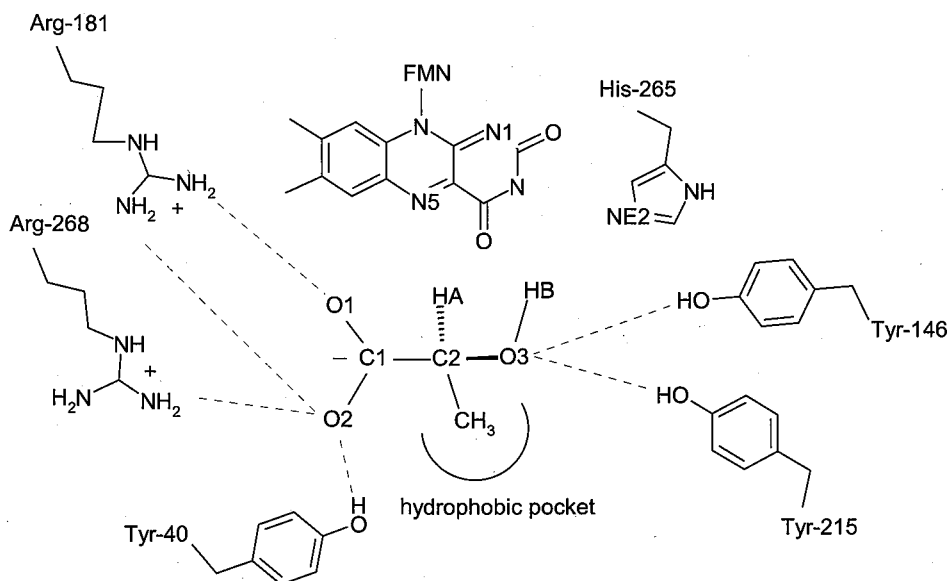
Fig. 25 A predicted structure of L-lactate in the active site of LOX. The simulated L-lactate was adjusted with its surround geometrical restraint. These dotted lines indicate hydrogen bonds and salt-bridges between the model L-lactate molecule and the LOX amino acid residues. Predicted hydrogen atoms (blue) were located near N5 atom of FMN and NE2 atom of His-265.
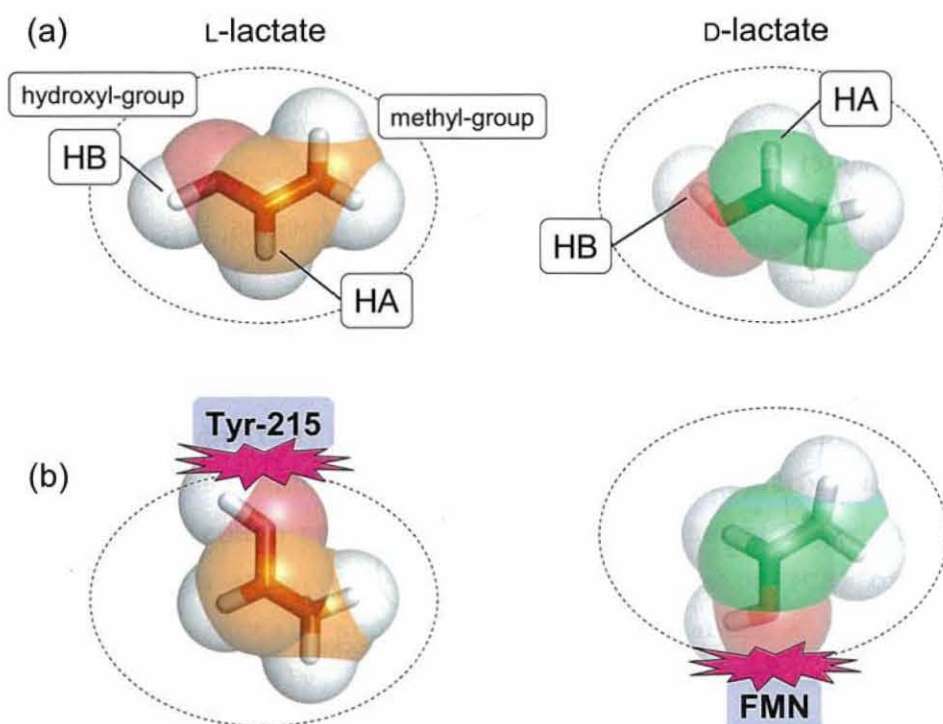
Fig. 26 The schematics of the model D/L-lactate located in the active site. The view of D/L-lactate from the carboxyl-group and each atoms are colored respectively: carbon (orange/green), oxygen (red), nitrogen (blue) and hydrogen (white). The dotted lines indicate the range of active site cavity and the spheres indicate the van der Waals radius. (a) The model D/L-lactate molecules are placed in suitable positions, but the hydrogen atom (HA) of D-lactate is far away from FMN. (b) The model D/L-lactate molecules are in the bad arrangements with steric clashes. The arrangement of the model L-lactate is based on the carbanion mechanism. The model D-lactate is placed Based on the arrangement of the model L-lactate where the position of hydrogen atom (Cα-H) interchanges to the position of hydroxyl group (Cα-OH).

(a) The model L-lactate
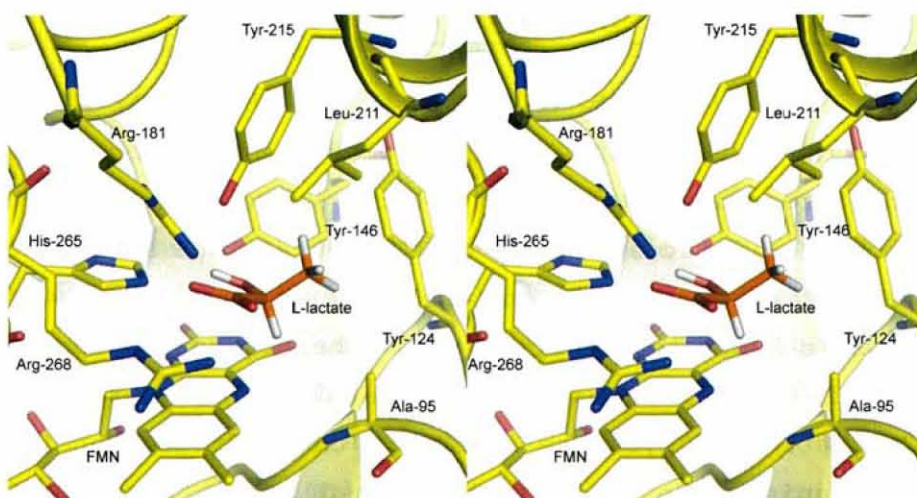
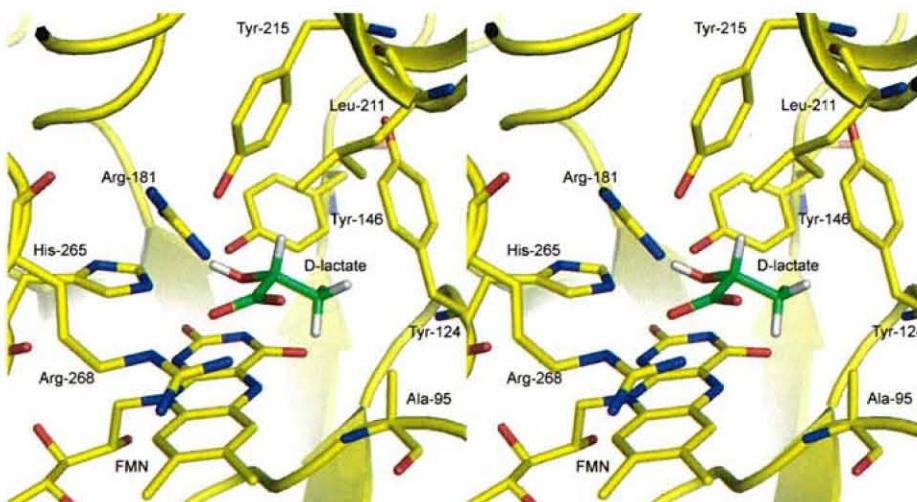
(b) The model D-lactate

Fig. 27   The stereo view of the active site in LOX in the simulation of placing the model L-lactate (a) and D-lactate (b) which are colored with green and orange respectively.

71

CHAPTER 4: DISCUSSION

The substrate specificity and reductive half-reaction mechanism were noted from the characteristic structure of LOX between the substrate and active site residues. The substrate specificity of LOX is known to be narrow than other lactate oxidase. It is conceivable that the catalysis of L-lactate oxidation to pyruvate reacts in the hydride transfer mechanism. They seem to be caused by the structural limitation at its active site. We discuss these mechanisms in the following sections.

4.1 Substrate specificity

It have been reported that LOX has high enzymatic activity for L-lactate as substrate, but very low activity for D-lactate, 2-hydroxy butyrate and L-mandelate (Duncan, J. D., 1989; Yorita, K., et al., 1996). The substrate specificity of LOX was clearly elucidated by specific interactions between the substrate and the enzyme as described in the previous section. The tight interactions must restrain the conformation of the substrate molecule and the variety of the substrate molecule.

Especially, the confined structure of the hydrophobic pocket contributes mainly to the substrate specificity. The members of the hydrophobic pocket components, Trp-108 in GOX and Ala-95 in LOX, have been reported about the changes of the oxidase activities with point mutations (**Fig. 28**).
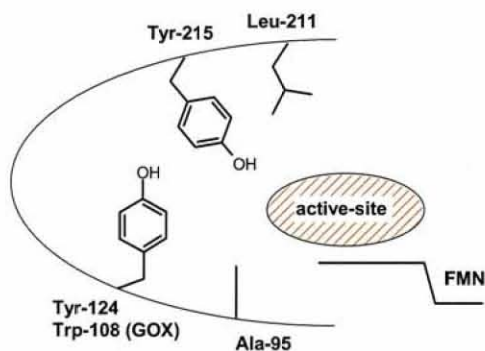
Fig. 28 The schematics of the hydrophobic pocket in LOX. Tyr-124 and Ala-95 compose the lower structure of the pocket and Tyr-215 and Leu-211 makes the upper structure.

73

The structural comparison with family enzymes showed that the residue corresponding to Tyr-124 of LOX were not conserved in amino acid sequence, Trp-108 in GOX, Leu-230 in FB2 and Tyr-107 in LCHAO, but they were located in the similar positions respectively (**Fig. 16**). Stenberg, K., et al. has revealed that the Trp-108 in GOX is involved in determining the substrate specificity by the mutagenesis experiments of Tryptophan to serine. The substitution of the rather bulky and hydrophobic tryptophan residue (Trp-108) by a small and hydrophilic serine residue (serine) causes dramatic effects on both the Michaelis constant (K_m) and turnover number (k_{cat}) of larger substrates, L-lactate, DL-2-hydroxy butyrate and L-mandelate, than glycolate (Stenberg, K., et al., 1995).

The previous mutagenesis experiment of Ala-95 to glycine of LOX has been shown that its oxidase activity increases with longer chain α-hydroxy acids (α-hydroxy butyrate and α-hydroxy valerate) and aromatic α-hydroxy acid (L-mandelate) (Yorita K. et al., 1997).

From these mutagenesis reports, there were common effects that both k_{cat} and K_m were increased by these point mutations. In other words, it was revealed that these mutations enhanced their catalytic activity, but decreased the affinity for a substrate. Therefore, the structure of hydrophobic pocket including both Ala-95 and Tyr-124 is important to determine the substrate specify.

In this study, the characteristic hydrophobic pocket in LOX is the most important feature to understand the enzymatic activity because the hydrophobic pocket is narrowed by this structure composed of Tyr-215 and Leu-211. These residues (Tyr-215 and Leu-211) seem to restrain the free movement of substrate molecule; the rotation around the C1-C2 axis and the translational motion above the flavin-ring (**Fig. 29**). We consider that these structural limitations affect the high substrate specificity of LOX for a L-lactate because its active site cavity is suitable for the L-lactate, not for the longer chain or aromatic hydroxy acid, by the space of its hydrophobic pocket.
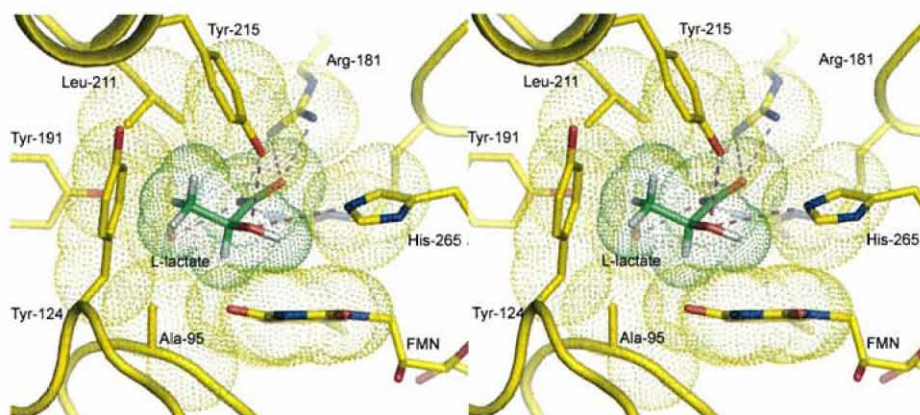
Fig. 29 The stereo view of the active site components containing the model L-lactate. The dotted spheres indicate the van der Waals radius. Oxygen (red), nitrogen (blue) and hydrogen (white) are colored respectively. The bound model L-lactate is colored in green and the atom of residues, which are indicated by dotted spheres, within a radius of 4 Å from lactate are colored in yellow. The dotted line (magenta) indicates hydrogen bonds.
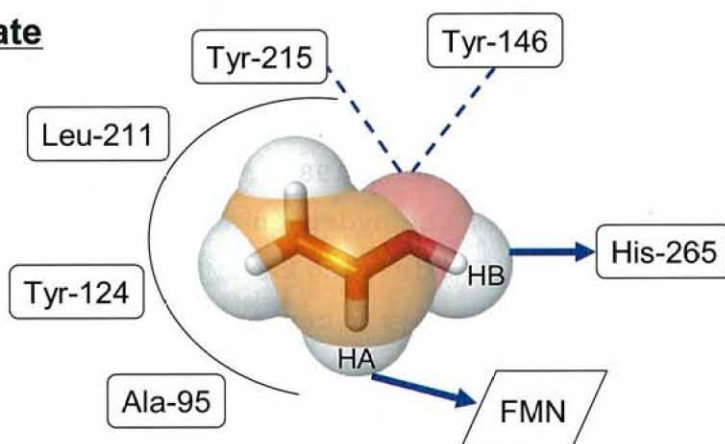
Specificity of Optical isomers, D/L-lactate

In LOX, it has been reported that D-lactate molecule is not oxidized, but it affects as competitive inhibitor (Duncan, J.D., et al., 1989). In the simulation of the model D-lactate, the hydrogen atom (HA) was located far away from the flavin-ring of FMN molecule and His-265 residue as the catalytic centers (**Fig. 30**). The hydroxyl group of the model D-lactate was in the range of hydrogen bond interaction with two tyrosine residues (Tyr-215 and Tyr-146) and its methyl group could be placed into the hydrophobic pocket. Thus, the model D-lactate is bound rigidly at the active site, but it is located in the position where it is difficult to dehydrogenize the hydrogen atom (HA) by FMN. Therefore, the feature of D-lactate as the unreact substrate and competitive inhibitor is considered to be due to the arrangement of the hydrogen atom of D-lactate.

On the other hand, the simulation for the L-lactate complex showed that the model L-lactate was located in a suitable position for abstracting the proton of the hydroxyl-group by His-265 residue and the hydrogen atom (HA) is located in the geometrically suitable position for the lone-pair interaction with N5 atom of FMN no steric clash as described previously.

Therefore, the strict specificity of the chiral substrate is supposed by the rigid cavity and the particular arrangement of the catalytic bases to L-lactate conformation.

L-lactate

Tyr-215   Tyr-146

Leu-211

HB → His-265

Tyr-124

HA → FMN

Ala-95

D-lactate

Tyr-215   Tyr-146

Leu-211

HA

HB

His-265
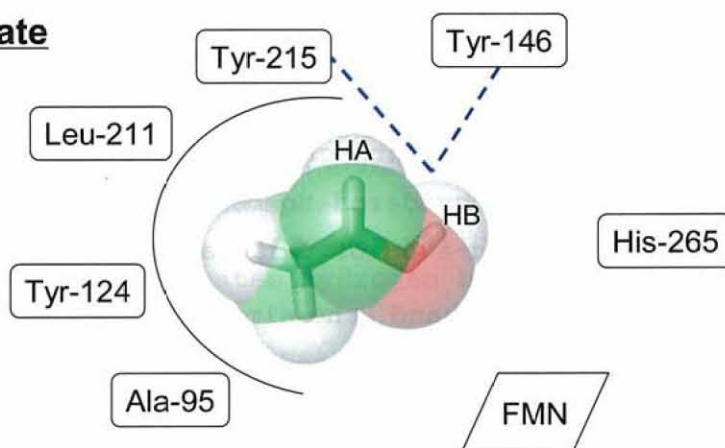
Tyr-124

Ala-95   FMN

Fig. 30 The schematics of bound D/L-lactate at the active site, which are the view from reverse of carboxyl-group of D/L-lactate. The spheres express the atoms of D/L-lactate; hydrogen (white), oxygen (red) and carbon (orange/green). Dotted lines and semi-circle line mean the hydrogen bonds and hydrophobic pocket respectively. The blue arrows represent the flow of abstracting hydrogen by His-265 and FMN as the catalytic base.

78

4.2 The suggestion of reductive half-reaction in LOX

The mechanism of abstracting protons

Based on the arrangement of active site residues around the lactate molecule, we propose the dehydrogenation mechanism of reductive half-reaction consistent with the hydride transfer mechanism (**Fig. 2**).

The substrate is fixed rigidly in the orientation, where the hydrogen of the hydroxyl-group (Cα-OH) is located near to NE2 atom of His-265 and the hydrogen atom (Cα-H) is closely located to the N5 atom of FMN molecule (**Fig. 29**). It may be concluded that the hydroxyl proton (Cα-OH) is abstracted by His-265 and α-proton (Cα-H) is transferred to the N5 position of FMN. This dehydrogenation mechanism is consistent of the hydride transfer mechanism. If we considered the dehydrogenation mechanism in LOX based on the carbanion mechanism, it would be structurally impossible to abstract protons because the hydroxyl-group is located in the steric clash to Tyr-215 residue (**Fig. 26 (b)**).

Therefore, the reductive half-reaction of LOX must proceed in hydride transfer mechanism. In other family, because this rotation of the substrate is relative easy in their loose active site cavities compared with LOX, it seems that two possibilities of the reaction mechanism (carbanion and hydride transfer mechanism) are in debate.

The reductive half-reaction scheme in LOX

Our suggestion about the reductive half-reaction consists of two reactions: the hydroxyl-group is dehydrogenized by His-265 residue and the hydrogen atom (Cα-H) is abstracted by FMN molecule. This mechanism belongs to the hydride transfer mechanism rather than the carbanion mechanism. This reaction steps are shown in (**Fig. 32**). The reaction mechanism is based on the characteristic arrangement of LOX, but this structure is helpful to understand the reaction mechanism of α-hydroxy acid oxidase.

In the initial step (a), L-lactate molecule moves into the inside through the cavity at the corner of tetramer and the substrate is fixed at the active site with the ionic interactions, hydrogen bonds and the hydrophobic interactions (**Fig. 22**).

In the second step (b), the hydroxyl group is attacked by His-265 as a catalytic base residue. The proton of hydroxyl group is transferred to NE2 position of His-265. The α-proton (Cα-H) is transferred to N5 position of FMN by the nucleophilic reaction. At the same time, a proton is transferred from Lys-241. Consequently (c), a pyruvate is generated and the FMN is reduced by accepting hydrogen atoms at N5 and N1 positions (**Fig. 31**).

After the dehydrogenation of L-lactate, the FMN is electrically stabilized by accepting the proton from basic residue Lys-241 which is located near the N1 atom

80

of FMN within average 2.9 Å and the reduced His-265 is stabilized by acidic residue Asp-174 which is located within average 2.9 Å (**Fig. 31**). These residues, Lys-241 and Asp-174, as electric stabilizers are highly conserved in family enzymes.
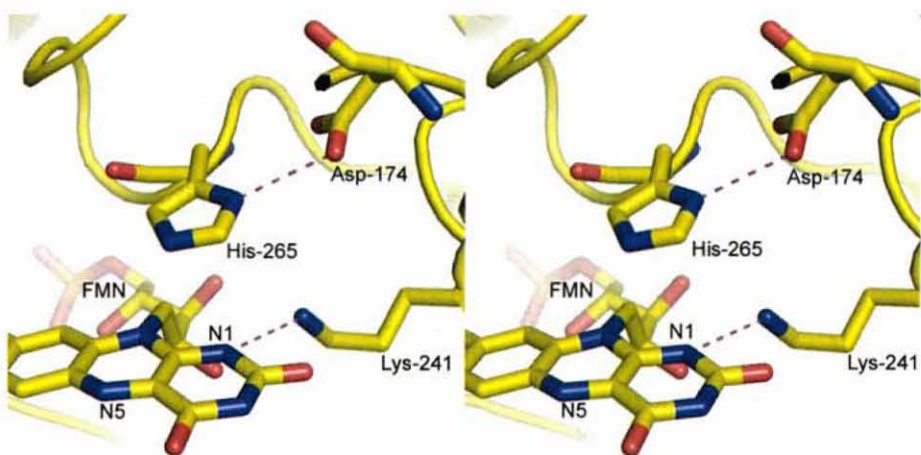

Fig. 31 The stereo view of the interaction between proton accepters and charge residues stabilizing them. Their gap distances are less than 3 Å respectively and their residues (Asp-174 and Lys-241) are conserved in family enzymes structurally.
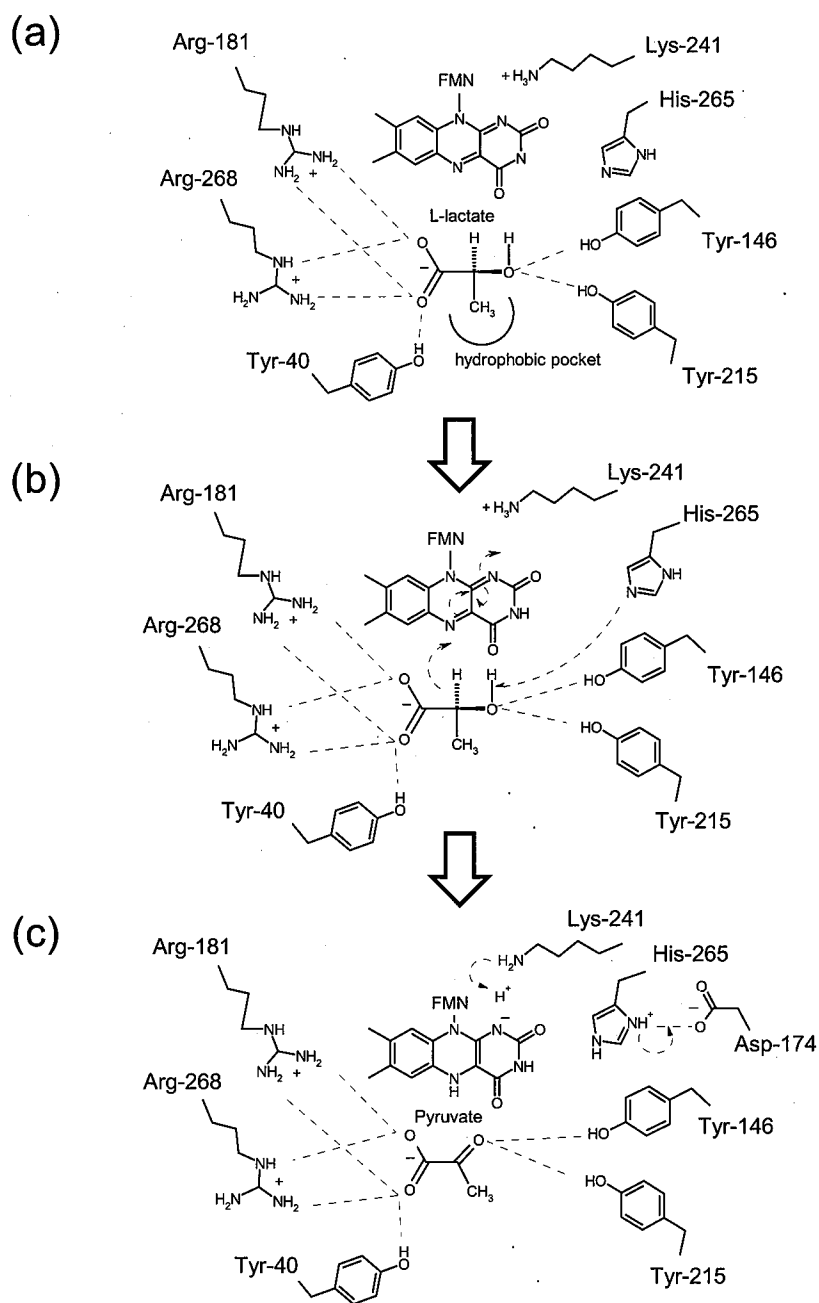
Fig. 32 Reductive half-reaction scheme in LOX based on hydride transfer mechanism.

After the dehydrogenation reaction

The reduced FMN is reoxidized by molecular oxygen in oxidative half-reaction (**Fig. 3**). The electrons and protons are transferred to molecular oxygen and a hydrogen peroxide is generated. This reaction has been generally accepted as a common mechanism in flavoenzymes. The reduced FMN interacts more repulsively with the negative charge of the pyruvate than the oxidized FMN. Thus, the product, pyruvate, is pushed out by molecular oxygen.

The examination of the kinetic pathway for LOX have reported that the pathway is a variation of the classical ping-pong mechanism, in which the second substrate, molecular oxygen, does not form a detectable Michaelis complex, reacting in a second order fashion with reduced enzyme to return it to its oxidized form, ready for the next cycle of its catalysis (Maeda-Yorita, K., et al., 1995).

CHAPTER 5: CONCLUSION

We have revealed these results from the study about LOX based on the structural analysis.

1) We determined the crystal structure of native LOX (2.07 Å) and LOX-pyruvate complex (1.9 Å). Our determined structures are clearly observed overall compared with other family enzymes (FB2, GOX and LCHAO), which have some lacked segments in long-loop structure covering the active site cavity.

2) We found the substrate specificity of LOX with the specific arrangement of active site residues, which limit the structure of its substrate with the narrow hydrophobic pocket. LOX seems to select the preferable optical isomer based on the arrangement of the catalytic centers (FMN and His-265) in the narrow active site cavity.

3) We suggested the reductive half-reaction in LOX based on the characteristic motif of binding a substrate molecule. It is classified to the hydride transfer mechanism. The characteristic motif is reasonable to understanding this dehydrogenation mechanism in contrast to the structure of other family enzymes. We could clearly suggest the reductive half-reaction mechanism in LOX as hydride transfer reaction. This structure is helpful to understand the reaction mechanism of α-hydroxy acid oxidase.

REFERENCE

Banner, D.W., Bloomer, A.C., Petsko, G.A., Phillips, D.C., Pogson, C.I., Wilson, I.A., Corran, P.H., Furth, A.J., Milman, J.D., Offord, R.E., Priddle, J.D. & Waley, S.G. Structure of chicken muscle triose phosphate isomerase determined crystallographically at 2.5 angstrom resolution using amino acid sequence data. *Nature* **255**, 609-614 (1975).

Brunger, A.T. Assessment of phase accuracy by cross validation: the free R value. Methods and applications. *Acta Crystallogr. D* **49**, 24-36(1993).

Brunger, A.T., Adams, P.D., Clore, G.M., DeLano, W.L., Gros, P., Grosse-Kunstleve, R.W., Jiang, J.S., Kuszewsk, i.J., Nilges, M., Pannu, N.S., Read, R.J, Rice, L.M., Simonson, T., & Warren, G.L. Crystallography & NMR system: A new software suite for macromolecular structure determination. *Acta Crystallogr. D* **54**, 905-921(1998).

Collaborative Computational Project 4, The CCP4 suit: programs for protein crystallography. *Acta Crystallogr. D* **50**, 760-763(1994).

Cunane, L.M., Barton, J.D., Chen, Z.W., Le, K.H., Amar, D., Lederer, F., & Mathews, F.S. Crystal structure analysis of recombinant rat kidney long chain hydroxy acid oxidase. *Biochemistry* **44**, 1521-1531(2005).

Dancan, J.D., Wallis, J.O. & Azari, M.R. Purification and properties of Aerococcu viridans lactate oxidase. *Biochem. Biophys. Res. Commun.* **164**, 919-926(1989).

Diep Le, K.H. & Lederer, F. Amino acid sequence of long chain alpha-hydroxy acid oxidase from rat kidney, a member of the family of FMN-dependent alpha-hydroxy acid-oxidizing enzymes. *J. Biol. CHem.* **266**, 20877-20881(1991).

Dubois, J., Chapman, S.K., Mathews, F.S., Reid, G.A. & Lederer, F. Substitution of Tyr254 with Phe at the Active site of Flavocytochrome b2: Consequences on Catalysis of Lactate Dehydrogenation. *Biochemistry* **29**, 6393-6400(1990).

Emsley, P. & Cowtan, K. COOT: model-building tools for molecular graphics. *Acta Crystallogr. D* **60**, 2126-2132(2004).

Fitzpatrick, P. F. Carbanion versus hydride transfer mechanisms in flavoprotein-catalyzed dehydrogenations. *Bioorg. Chem.* **32**, 125-139(2004).

Ghsala, S. & Massy, V. L-lactate oxidase in Chemistry and Biochemistry of Flavoenzymes. *CRC Press, Boca, Raton, FL* **2**, 243-289(1991).

Laskowski, R.A., MacArthur, M.W., Moss, D.S. & Thornton, J.M. PROCHECK: a program to check the stereochemical quality of protein structures. *J. Appl. Crystallogr.* **26**, 283-291(1993).

Lederer, F. Flavocytochrome in Chemistry and Biochemistry of Flavoenzymes. *CRC Press, Boca Raton, FL* **2**, 152-242(1991).

Lennon, B.W., Williams, C.H. & Jr, Ludwig, M.L. Crystal structure of reduced thioredoxin reductase from Escherichia coli: structural flexibility in the isoalloxazine ring of the flavin adenine dinucleotide cofactor. *Protein Sci.* **8**, 2366-2379(1999).

Lindqvist, Y. Refined structure of spinach glycolate oxidase at 2 Å resolution. *J. Mol. Biol.* **209**, 151-166(1989).

Lindqvist, Y., Branden, C.I., Mathews, F.S. & Lederer, F. Spinach Glycolate Oxidase and Yeast Flavochytochrome b2 are Structurally Homologous and Evolutionaily Related Enzymes with Dstinctly Different Function and Flavin Mononucleotide Binding. *J. Biol. Chem.* **266**, 3198-3207(1991).

Maeda-Yorita, K., Aki, K., Sagai, H., Misaki, H. & Massey, V. L-lactate oxidase and L-lactate monooxygenase: mechanistic variations on a common structural theme. *Biochimie.* **77**, 631-642(1995).

McRee, D.E. Practical Protein Crystallography. *Academic Press, New York* (1993).

Morimoto, Y., Yorita, K., Aki, K., Misaki, H. & Massey, V. L-lactate oxidase from Aerococcus viridans crystallized as an octamer. Preliminary X-ray studies. *Biochimie.* **80**, 309-312(1998).

Moustafa, I.M., Foster, S., Lyubimov, A.Y & Vrielink, A. Crystal structure of LAAO from Calloselasma rhodostoma with an L-phenylalanine substrate: insights into structure and mechanism. *J. Mol. Biol.* **364**, 991-1002(2006).

Murshudov, G.N., Vagin, A.A. & Dodson, E.J. Refinement of macromolecular structures by the maximum-likelihood method. *Acta Crystallogr. D* **53**, 240-255(1997).

Otwinowski, Z. & Minor, W. Processing of X-ray diffraction data collected by oscillation methods. *Methods Enzymol.* **276**, 307-326(1997).

Sergio, A., Streitenberger, J.A., Lopez, M., Alvero, S.F. & Francisco, G.C. A Study on the Kinetic Mechanism of Apoenzyme Reconstitution from Aerococcus Viridans Lactate Oxidase. *J. Enz. Inhib.* **18**, 285-288(2003).

Smekal, O., Yasin, M., Fewson, C.A., Reid, G.A. & Chapman, S. K. L-mandelate dehydrogenase from Rhodotorula graminis: comparisons with the L-lactate dehydrogenase (flavocytochrome b2) from Saccharomyces cerevisiae. *Biochem J.* **15**, 103-107(1993).

Stenberg, K., Clausen, T., Lindqvist, Y. & Macheroux, P. Involvent of Tyr24 and Trp108 in substrate binding and substrate specificity of glycolate oxidase. *Eur. J. Biochem.* **228**, 408-416(1995).

Urban, P., Chirat, I. & Lederer, F. Rat kidney L-2-hydroxyacid oxidase. Structural and mechanistic comparison with flavocytochrome b2 from baker's yeast. *Biochemistry* **27(19)**, 7365-7371(1988).

Xia, Z.-X., Shamala, N., Bethge, P.H., Lim, L.W., Bellamy, H.D., Xuong, N.H., Lederer, F. & Mathews, F. S. Three-dimensional structure of flavocytochrome b2 from baker's yeast at 3.0 Å resolution. *Proc. Netl. Acad. Sci.* **84**, 2629-2633(1987).

Yorita, K., Matsuoka, T., Ballou, D. P., & Fukui, K. H265Q L-Lactate Oxidase from Aerococcus viridans. *Flavins and Flavoproteins* 37-41(2005).

LIST OF PUBLICATIONS

Umena, Y., Yorita, K., Matsuoka, T., Kita, A., Fukui, K. & Morimoto, Y. The crystal structure of L-lactate oxidase from Aerococcus viridans at 2.1 Å resolution reveals the mechanism of strict substrate recognition. *Biochem Biophys Res Commun.* **350(2)**, 249-56 (2006)

Umena, Y., Yorita, K., Matsuoka, T., Abe, M., Kita, A., Fukui, K., Tsukihara, T. & Morimoto, Y. Crystallization and preliminary X-ray diffraction study of L-lactate oxidase (LOX), R181M mutant, from Aerococcus viridans. *Acta Crystallogr. F* **61**, 439-41 (2005)